Supporting Information for:

Copper(II) complexes of macrocyclic and open-chain pseudopeptidic ligands: synthesis, characterization and interaction with dicarboxylates

Enrico Faggi,*[a] Raquel Gavara,[b] Michael Bolte,[c] Lluís Fajarí,[a] Luís Julià,[a] Laura Rodríguez[b] and Ignacio Alfonso*[a]

[a] Departamento de Química Biológica y Modelización Molecular, IQAC−CSIC, Jordi Girona, 16-26, E-08034 Barcelona, Spain.
[b] Departament de Química Inorgànica, Universitat de Barcelona, Martí i Franquès 1-11, E-08028 Barcelona, Spain
[c] Institut für Anorganische Chemie, J.-W.-Goethe-Universität, Max-von-Laue-Str.7, D-60438 Frankfurt/Main, Germany.

Table of Contents

1. Synthesis and Characterization of the ligands

L1

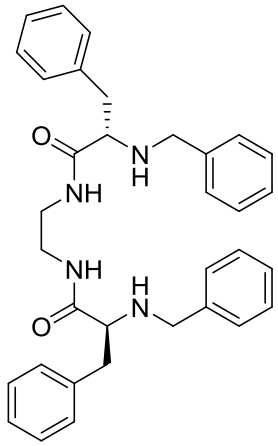

To a solution of **1** (360 mg, 1.01 mmol) in methanol (15 ml) was added benzaldehyde (454 µl, 4.46 mmol) and the resulting solution was stirred at room temperature during 6 hours. Sodium borohydride (470 mg, 12.2 mmol) was added in an ice bath that was later removed and the reaction mixture was stirred at room temperature during 16 hours. Aqueous 4M HCl was added, and a white solid formed. After 1 hour the solvents were evaporated at reduced pressure, affording a solid that was suspended in aqueous 4M NaOH. The product was extracted twice with DCM and once with AcOEt. Organic layers were combined, dried over $MgSO_4$ and concentrated at reduced pressure. The resulting thick oil was suspended in diethyl ether, triturated, filtered and washed with additional diethyl ether, affording **L1** as a white solid (440 mg, 0.82 mmol, 81% yield).
^{1}H-NMR (400 MHz, $CDCl_3$) δ 7.29 (bs, 2H), 7.26-7.15 (m, 12H), 7.12-7.09 (m, 4H), 7.05 (dd, *J* = 7.5, 1.9 Hz, 4H), 3.66 (d, *J* = 13.4 Hz, 2H), 3.48 (d, *J* = 13.4 Hz, 2H), 3.37-3.21 (m, 4H), 3.29 (dd, *J* = 9.1, 4.8 Hz, 2H), 3.13 (dd, *J* = 13.8, 4.7 Hz, 2H), 2.71 (dd, *J* = 13.8, 9.1 Hz, 2H), 1.65 (bs, 2H).
^{13}C-NMR (101 MHz, $CDCl_3$) δ 174.4, 139.2, 137.5, 129.3, 128.8, 128.6, 128.0, 127.3, 127.0, 63.2, 52.7, 39.5, 39.3.
HRMS (ESI-TOF) *m/z* [**L1** + H]$^+$ Calcd for ($C_{34}H_{39}N_4O_2$) 535.3073, found 535.3080.
IR (KBr, ν cm^{-1}): 3345, 3282, 1652, 1522, 745, 697.

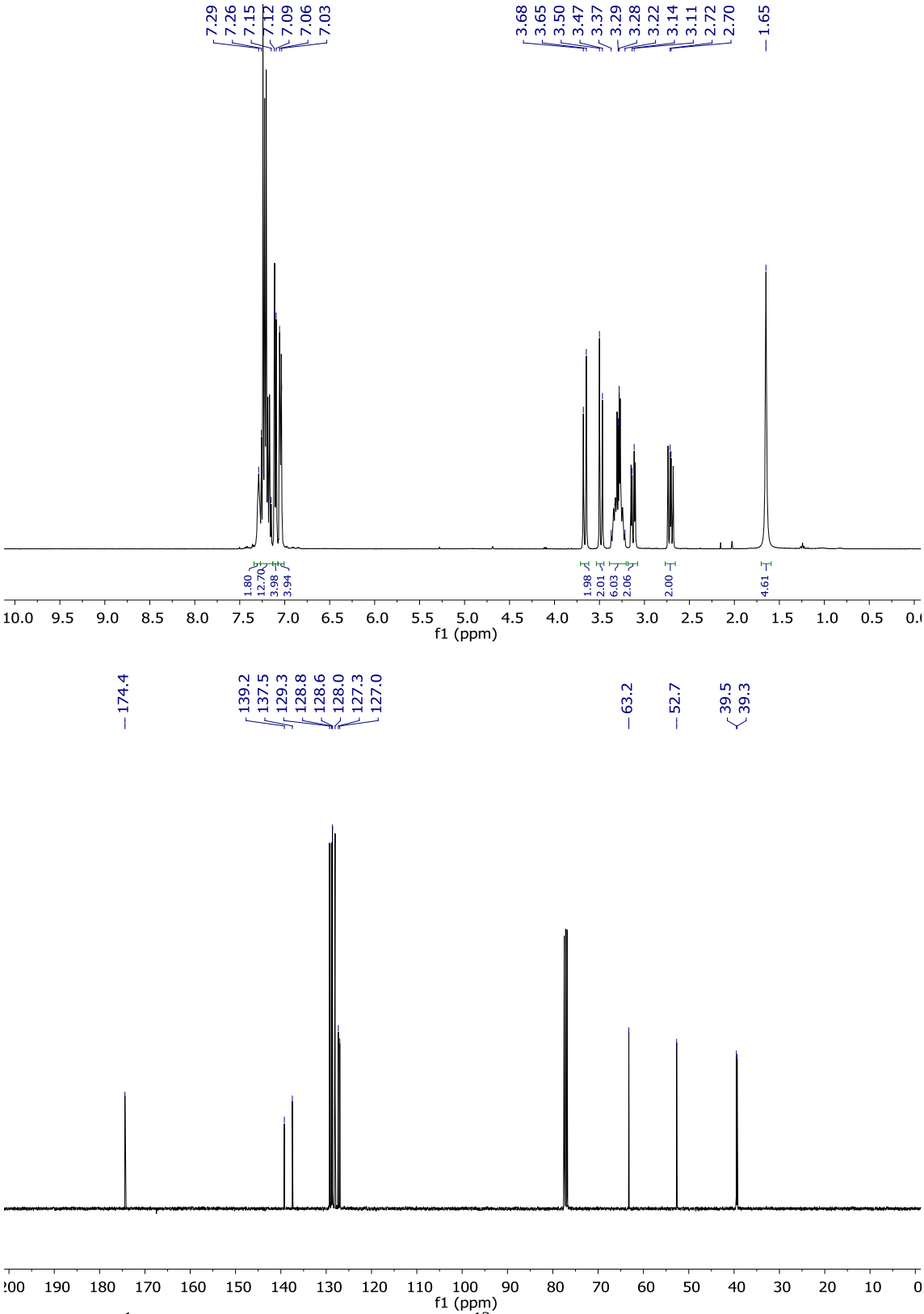

Figure S1. ^{1}H-NMR (400 MHz, $CDCl_3$) and ^{13}C-NMR (101 MHz, $CDCl_3$) spectra of **L1**.

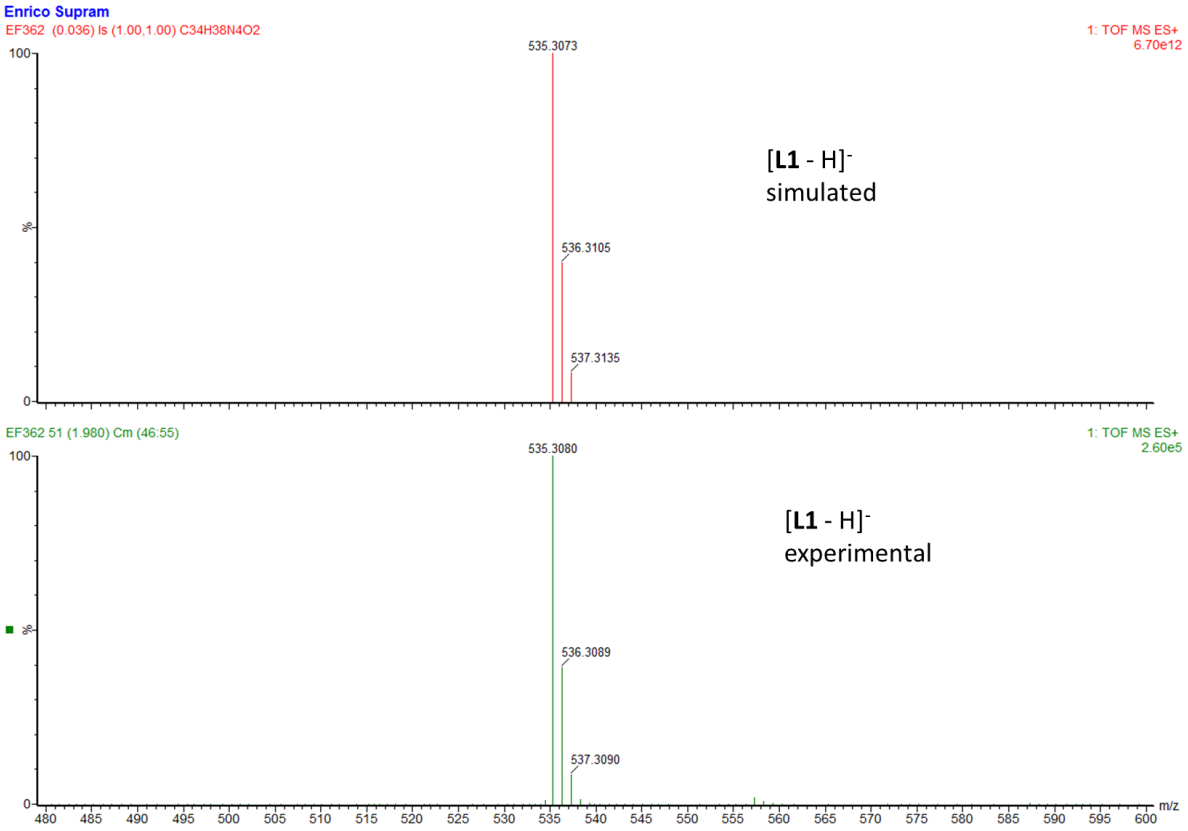

Figure S2. HRMS (ESI-TOF) spectrum of **L1**.

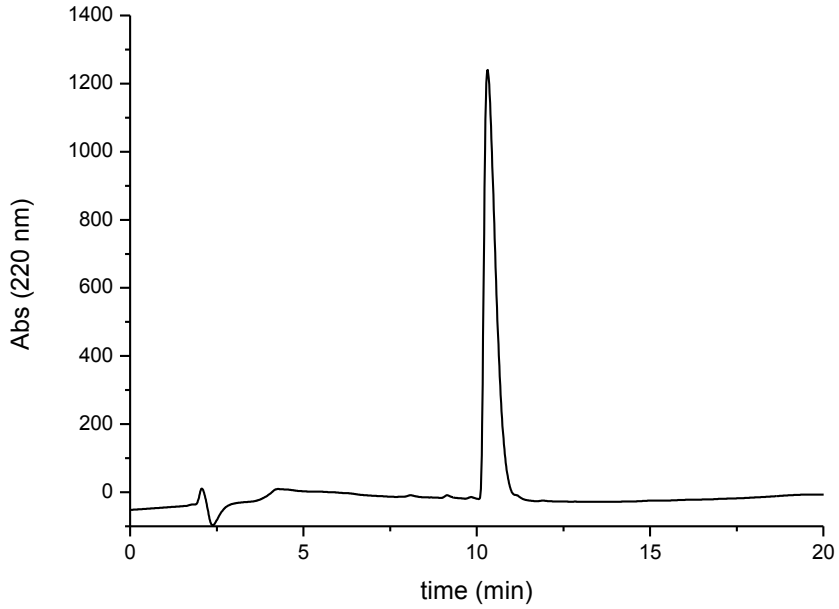

Figure S3. HPLC trace of **L1** (0% to 100% MeCN in water, in 20 min); t_R = 10.31.

L2

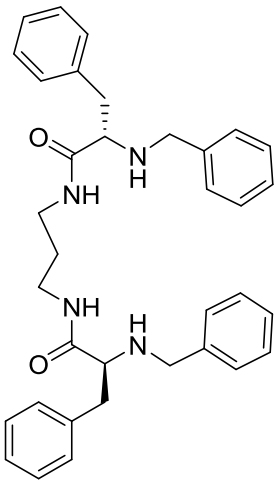

Obtained following the same procedure described for **L1**, using **2** (400 mg, 0.82 mmol) as starting material. **L2** was obtained as a waxy solid (240 mg, 0.82 mmol, 44% yield).
^{1}H-NMR (400 MHz, $CDCl_3$) δ 7.52 (t, *J* = 6.4 Hz, 2H), 7.35-7.18 (m, 12H), 7.14 (d, *J* = 6.6 Hz, 4H), 7.07 (d, *J* = 7.4 Hz, 4H), 3.70 (d, *J* = 13.4 Hz, 2H), 3.53 (d, *J* = 13.4 Hz, 2H), 3.36 (dd, *J* = 9.3, 4.4 Hz, 2H), 3.20-3.09 (m, 6H), 2.73 (dd, *J* = 13.8, 9.3 Hz, 2H), 1.75 (bs, 2H), 1.54 (p, *J* = 6.4 Hz, 2H).
^{13}C-NMR (101 MHz, $CDCl_3$) δ 174.0, 139.2, 137.4, 129.1, 128.7, 128.5, 128.0, 127.1, 126.8, 63.2, 52.6, 39.4, 35.6, 30.0.
HRMS (ESI-TOF) *m/z* [**L2** - H]$^-$ Calcd for ($C_{35}H_{39}N_4O_2$) 547.3073, found 547.3076.
IR (KBr, ν cm^{-1}): 3415, 3229, 1638, 1617, 1398.

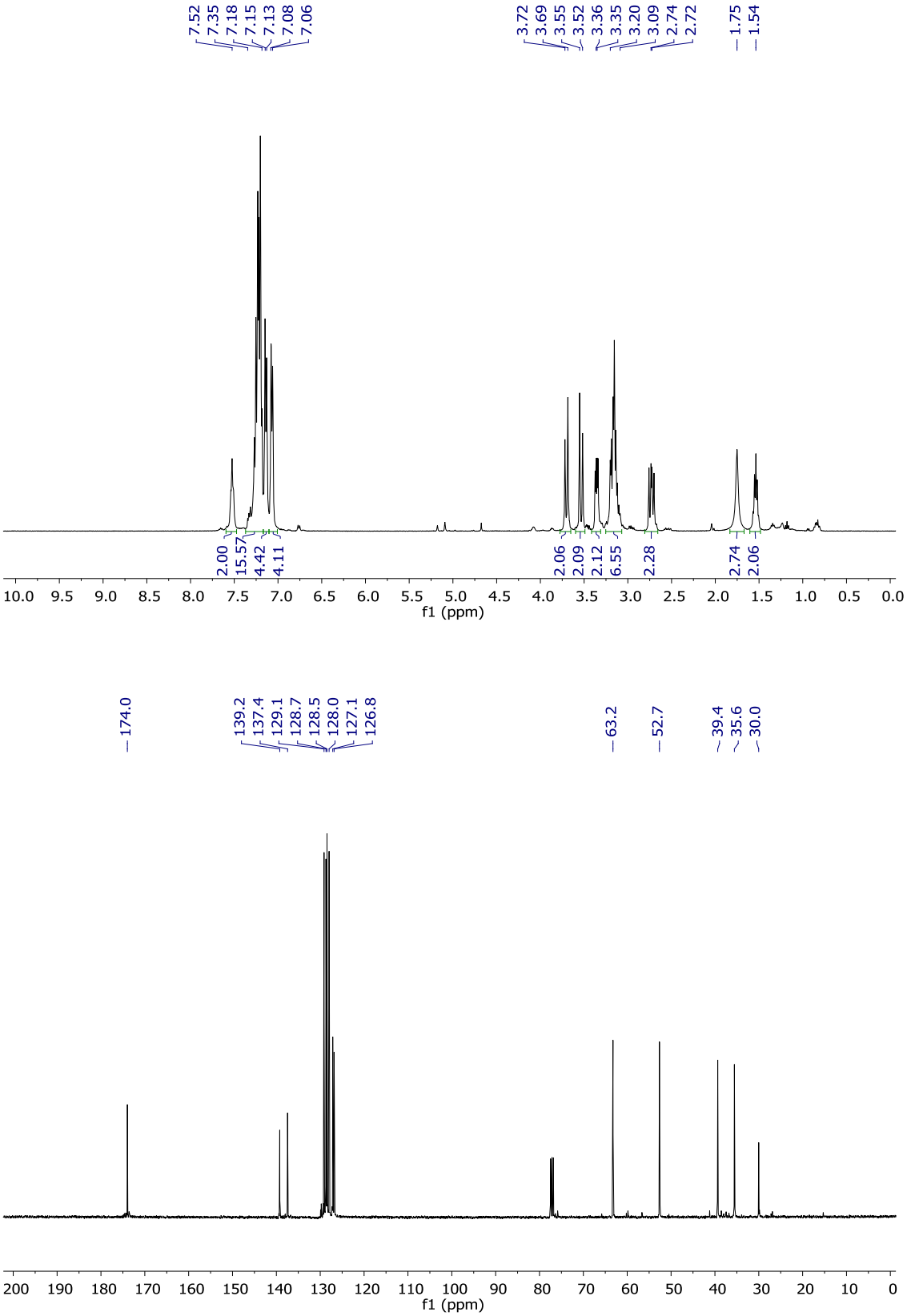

Figure S4. ^{1}H-NMR (400 MHz, $CDCl_3$) and ^{13}C-NMR (101 MHz, $CDCl_3$) spectra of **L2**.

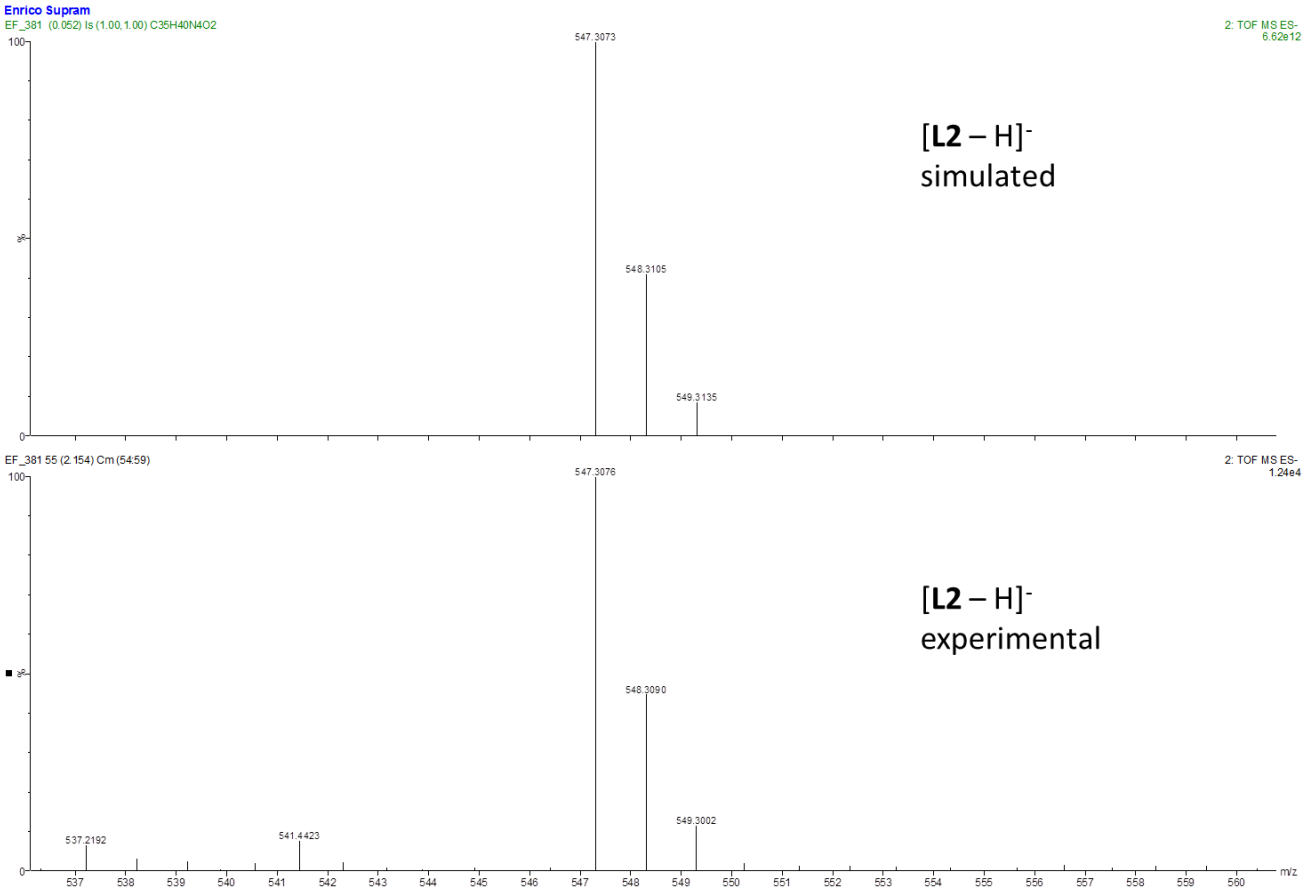

Figure S5. HRMS (ESI-TOF) spectrum of **L2**.

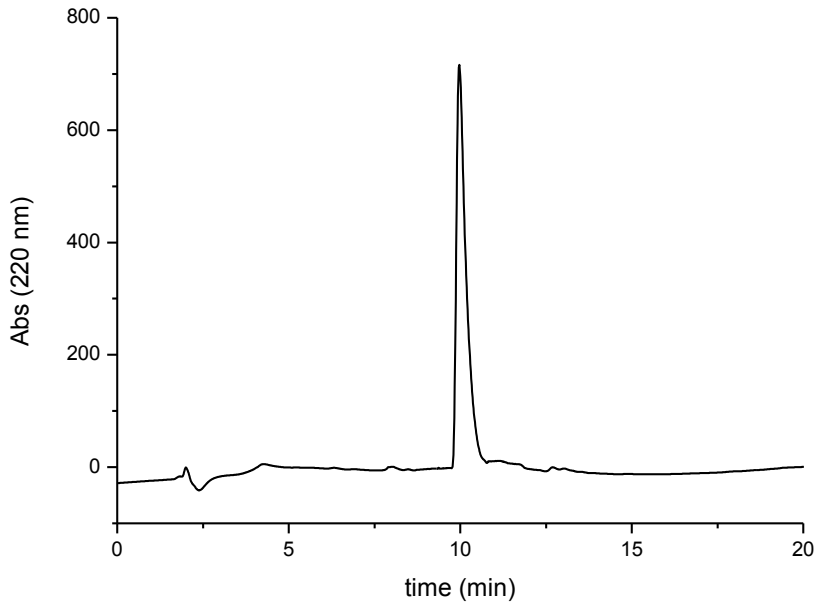

Figure S6. HPLC trace of **L2** (0% to 100% MeCN in water, in 20 min); t_R = 9.97.

L3

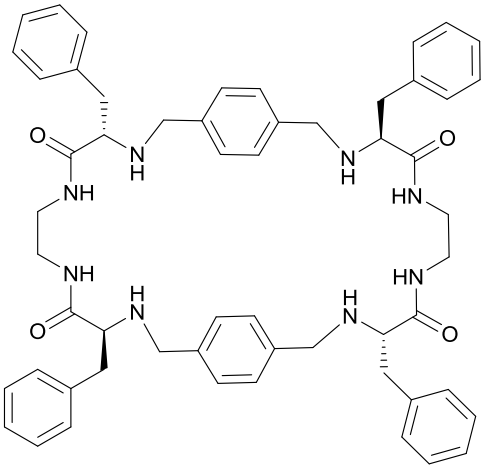

IR (KBr, ν cm^{-1}): 3415, 1653, 1521, 702.

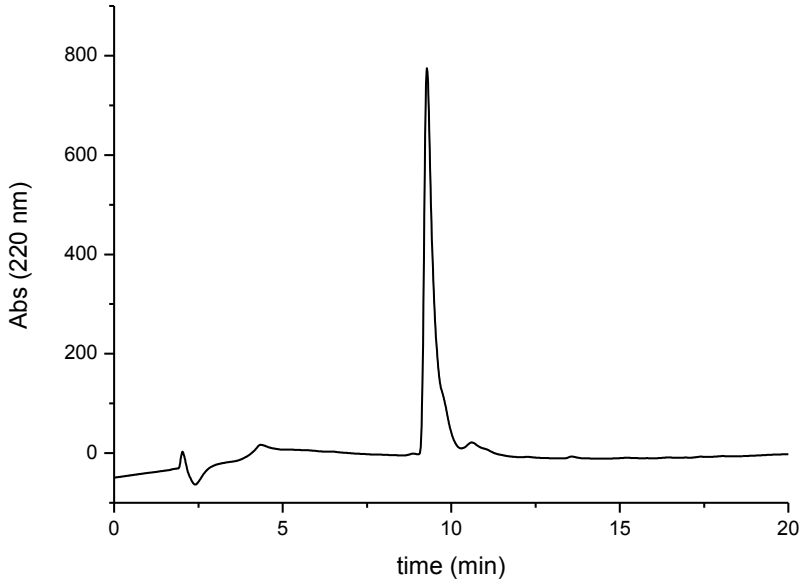

Figure S7. HPLC trace of **L3** (0% to 100% MeCN in water, in 20 min); t_R = 9.28.

L4

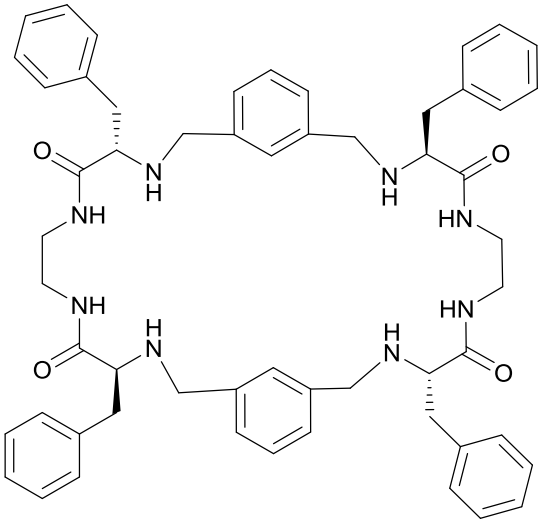

IR (KBr, ν cm^{-1}): 3417, 3232, 1643, 1520, 1397, 699.

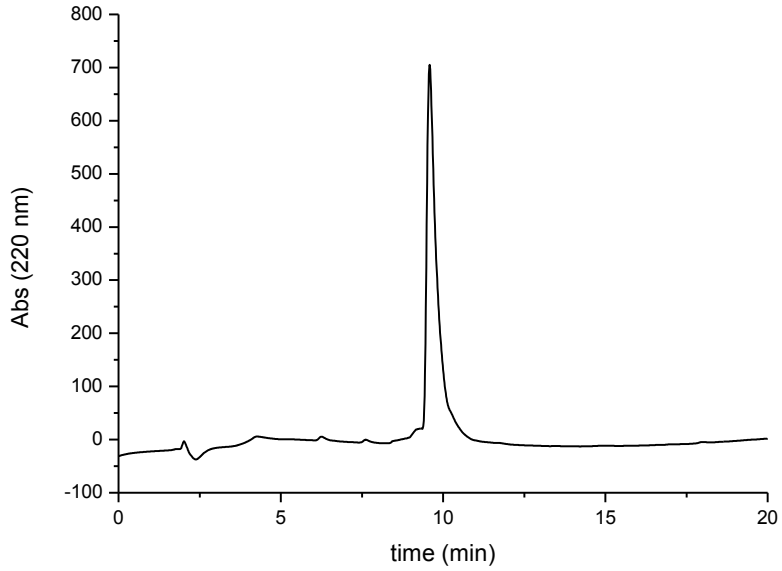

Figure S8. HPLC trace of **L4** (0% to 100% MeCN in water, in 20 min); t_R = 9.59.

2. Synthesis and Characterization of the Cu(II) complexes

CuL1

To a solution of **L1** (105 mg, 0.197 mmol) in MeOH (20 mL) were added $CuSO_4 \cdot 5H_2O$ (50 mg, 0.200 mmol) and NaOH (16 mg, 0.40 mmol). A colour change from blue to purple was observed. Reaction mixture was stirred during 30 minutes at room temperature and then centrifuged during 10 minutes. The white solid was discarded while the purple solution was concentrated at reduced pressure. Cu**L1** was obtained as a purple solid (94 mg, 0.157 mmol, 80% yield).

IR (KBr, ν cm^{-1}): 3406, 1598, 1454, 751, 700.

Elemental analysis: found: C: 64.75%, H: 5.93%; N: 8.75%; calculated for Cu**L1** + 2 H_2O; C: 64.59%, H: 6.38%, N: 8.86%.

CuL2

Prepared following the same procedure described for Cu**L1**. Cu**L2** was obtained as a pink solid. 76% yield.

IR (KBr, ν cm^{-1}): 3405, 3229, 1576, 1398.

Elemental analysis: found: C: 63.86%, H: 6.25%; N: 8.43%; calculated for Cu**L2** + 3 H_2O; C: 63.28%, H: 6.68%, N: 8.43%.

Cu_2L3

To a solution of **L3** (215 mg, 0.228 mmol) in MeOH (25 mL) were added $CuSO_4 \cdot 5H_2O$ (115 mg, 0.46 mmol) and NaOH (37 mg, 0.92 mmol). A colour change from blue to purple was observed. Reaction mixture was stirred during 30 minutes at room temperature and then centrifuged during 10 minutes. The white solid was discarded while the purple solution was concentrated at reduced pressure. Cu_2**L3** was obtained as a purple solid (175 mg, 0.164 mmol, 72% yield).

IR (KBr, ν cm^{-1}): 3404, 1599, 702.

Elemental analysis: found: C: 64.15%, H: 6.21%; N: 10.43%; calculated for: Cu_2**L3** + 1 H_2O; C: 63.80%, H: 5.93%, N: 10.63%.

Cu_2L4

Prepared following the same procedure described for Cu_2**L3**. Cu_2**L4** was obtained as a pink solid. 81% yield.

IR (KBr, ν cm^{-1}): 3414, 3229, 1614, 1397.

Elemental analysis: found: C: 63.75%, H: 5.95%; N: 10.38%; calculated for Cu_2**L4** + 1 H_2O; C: 63.80%, H: 5.93%, N: 10.63%.

HRMS Spectra of the Cu(II) Complexes

Cu**L1**

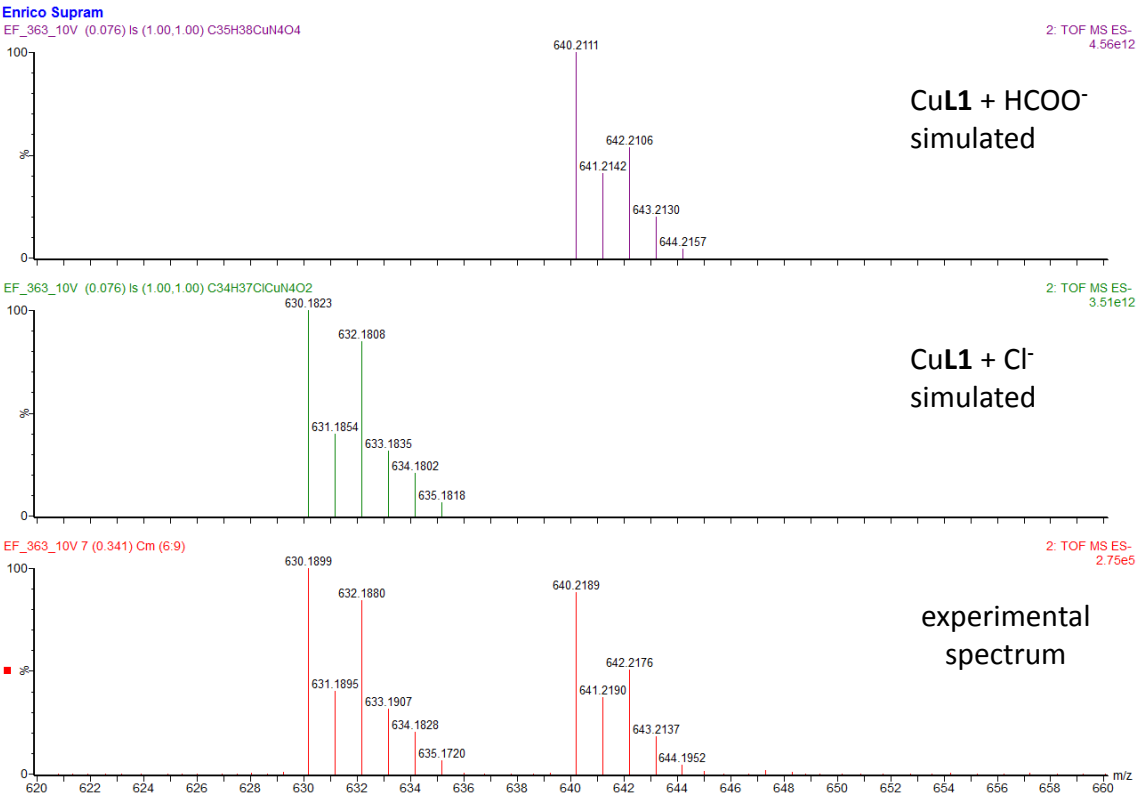

Figure S9. HRMS (ESI-TOF) spectrum of Cu**L1**.

Cu**L2**

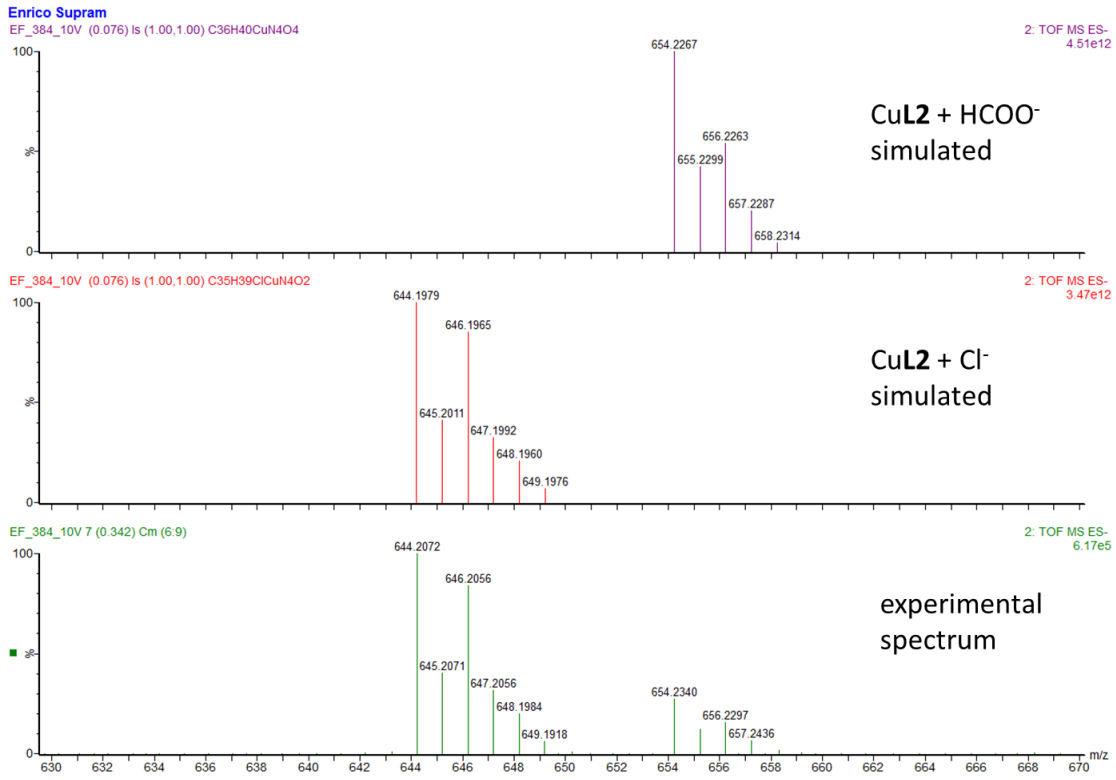

Figure S10. HRMS (ESI-TOF) spectrum of Cu**L2**.

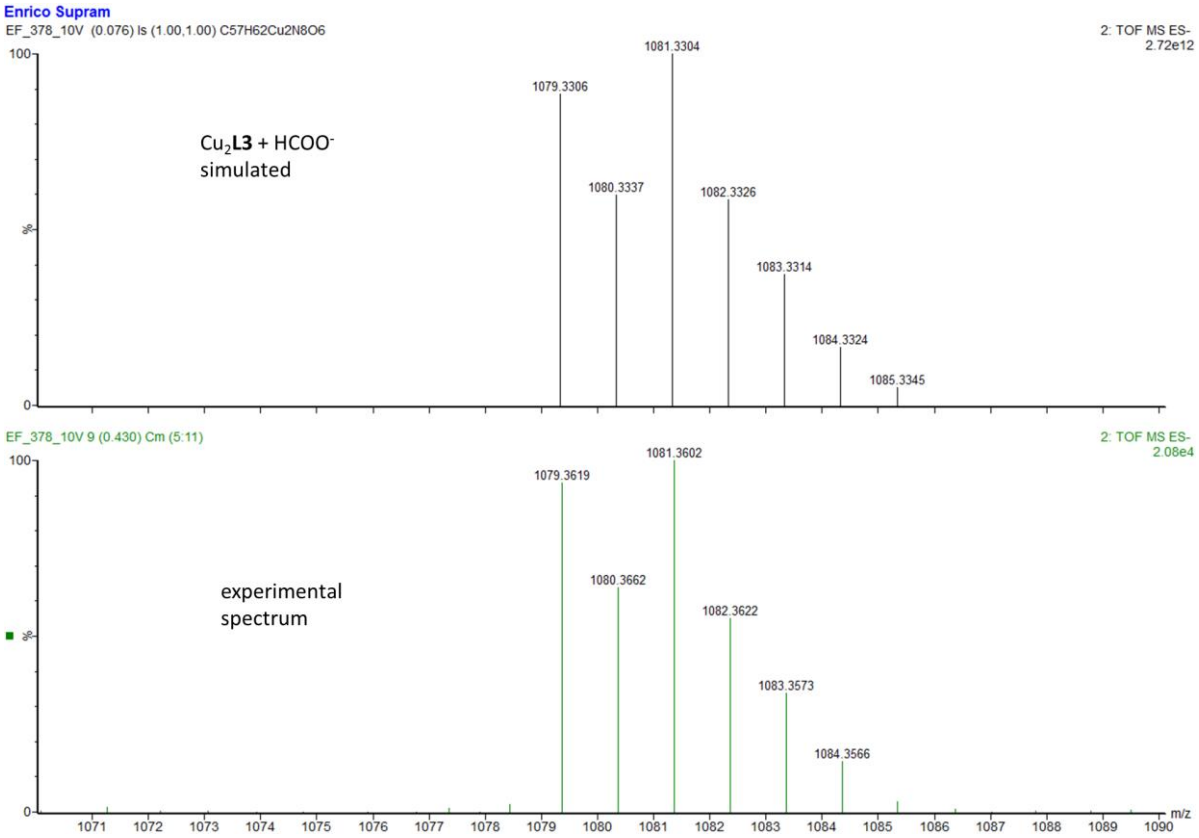

Figure S11. HRMS (ESI-TOF) spectrum of Cu_2**L3**.

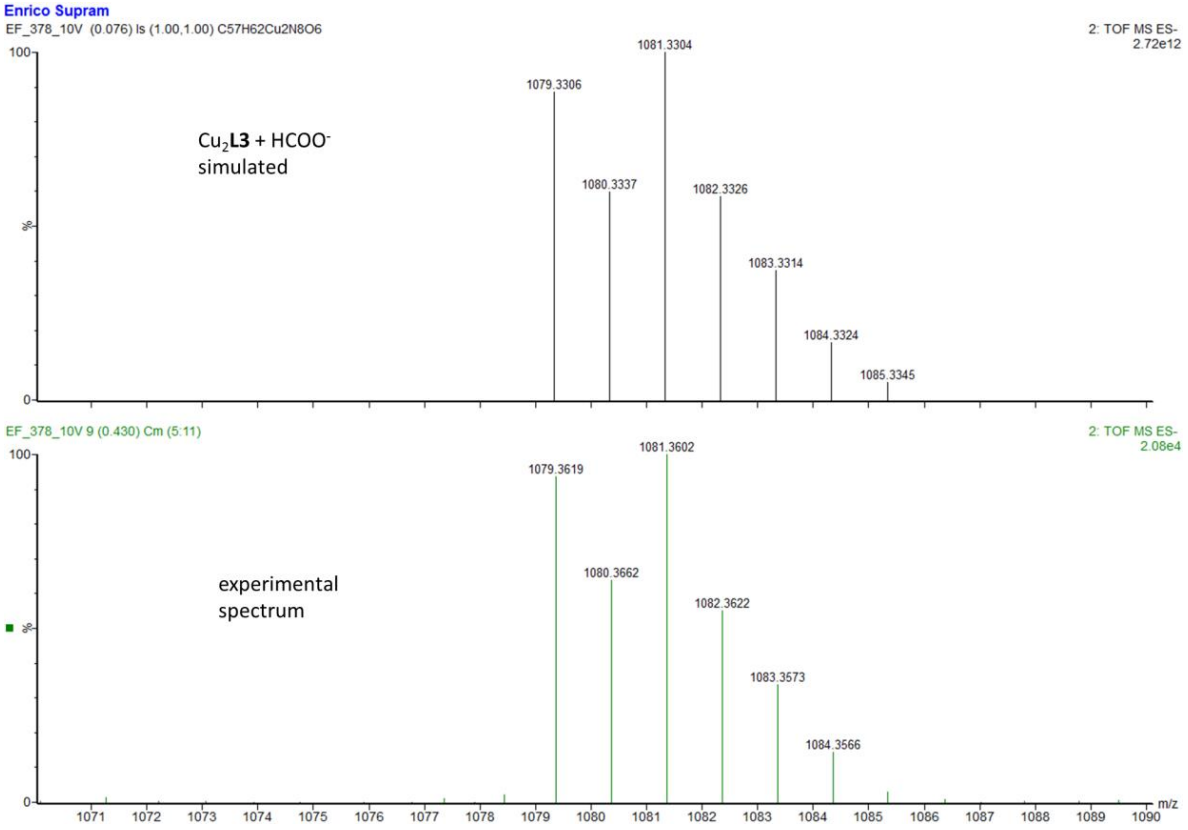

Figure S12. HRMS (ESI-TOF) spectrum of Cu_2**L4**.

UV-vis Spectra of the Cu(II) Complexes

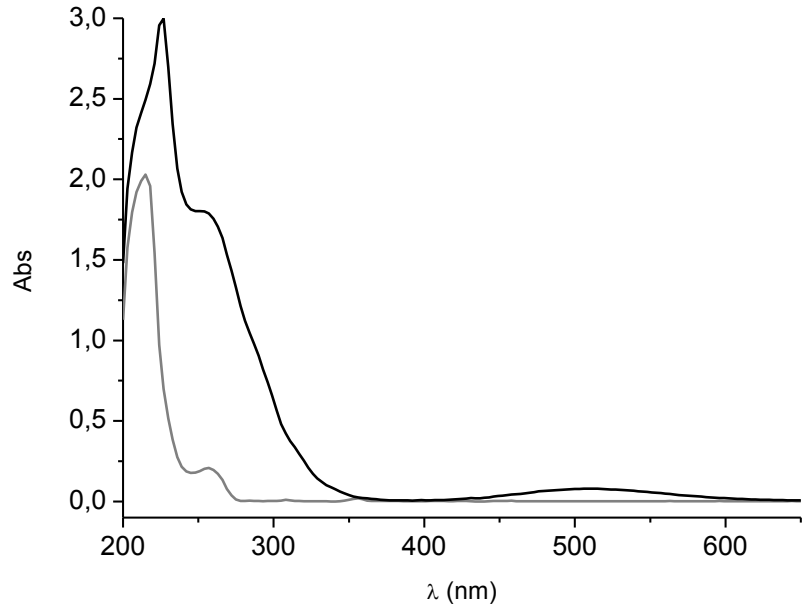

Figure S13. UV-vis spectra of Cu**L1** (black line) and **L1** (grey line) ($3.5 \cdot 10^{-4}$ M, MeOH).

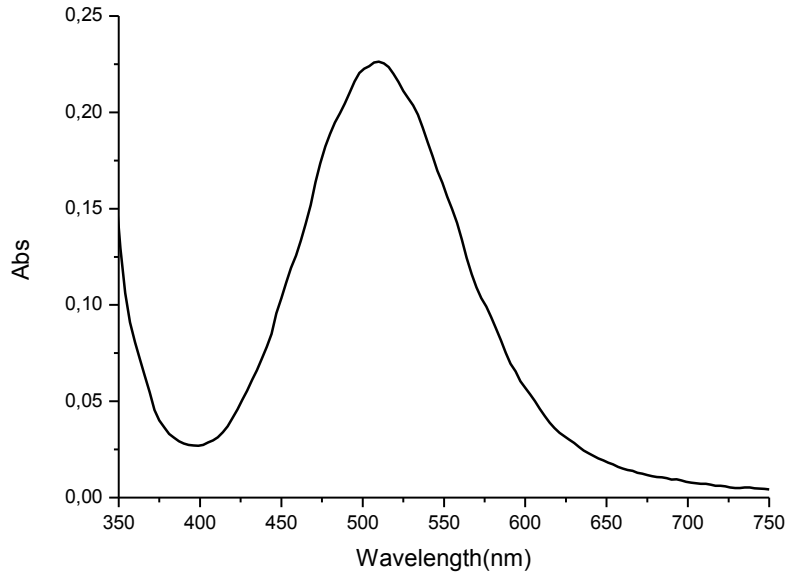

Figure S14. UV-vis spectrum of Cu**L1**, $1 \cdot 10^{-3}$ M, MeOH. (λmax = 510 nm; ε = 226 M^{-1} cm^{-1}).

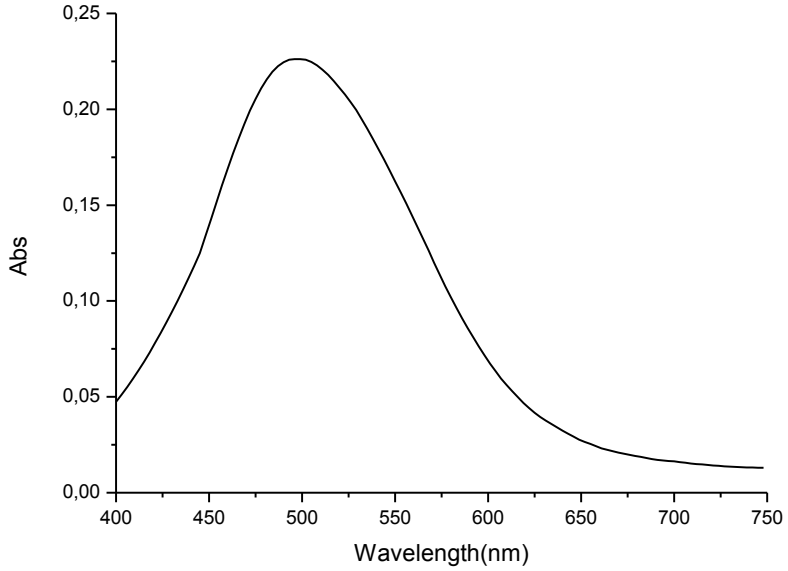

Figure S15. UV-vis spectrum of Cu**L2**, $2.4 \cdot 10^{-3}$ M, MeOH. (λmax = 498 nm; ε = 94 M^{-1} cm^{-1}).

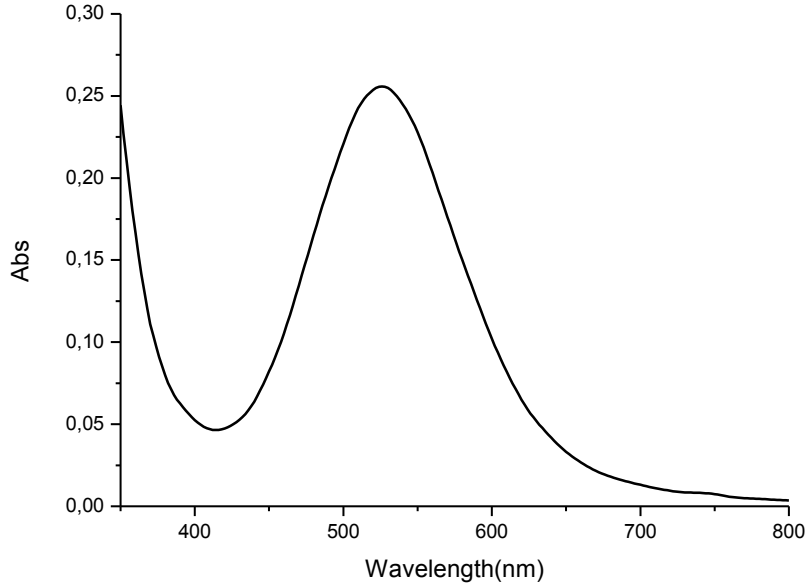

Figure S16. UV-vis spectrum of Cu_2**L3**, $7 \cdot 10^{-4}$ M, MeOH. (λmax = 526 nm; ε = 365 M^{-1} cm^{-1}).

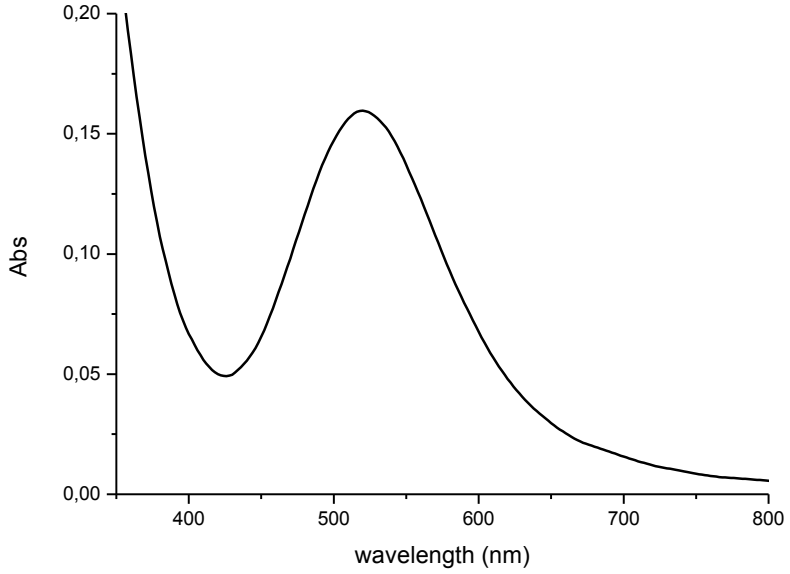

Figure S17. UV-vis spectrum of Cu_2**L4**, $5 \cdot 10^{-4}$ M, MeOH. (λmax = 519 nm; ε = 319 M^{-1} cm^{-1}).

3. IR spectra

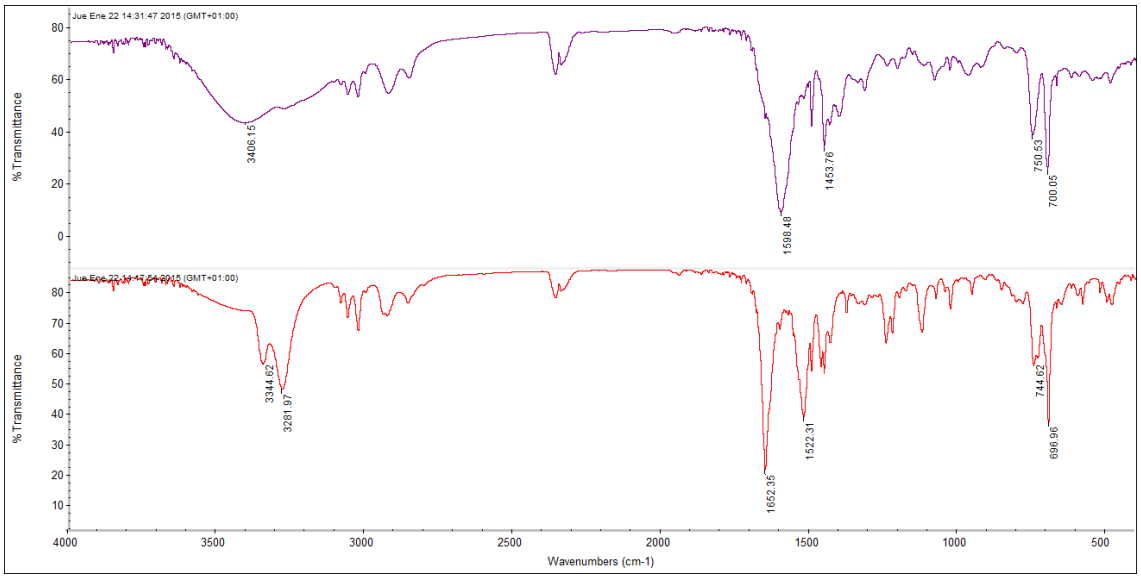

Figure S18. Infrared spectra of **L1** (red line) and Cu**L1** (purple line).

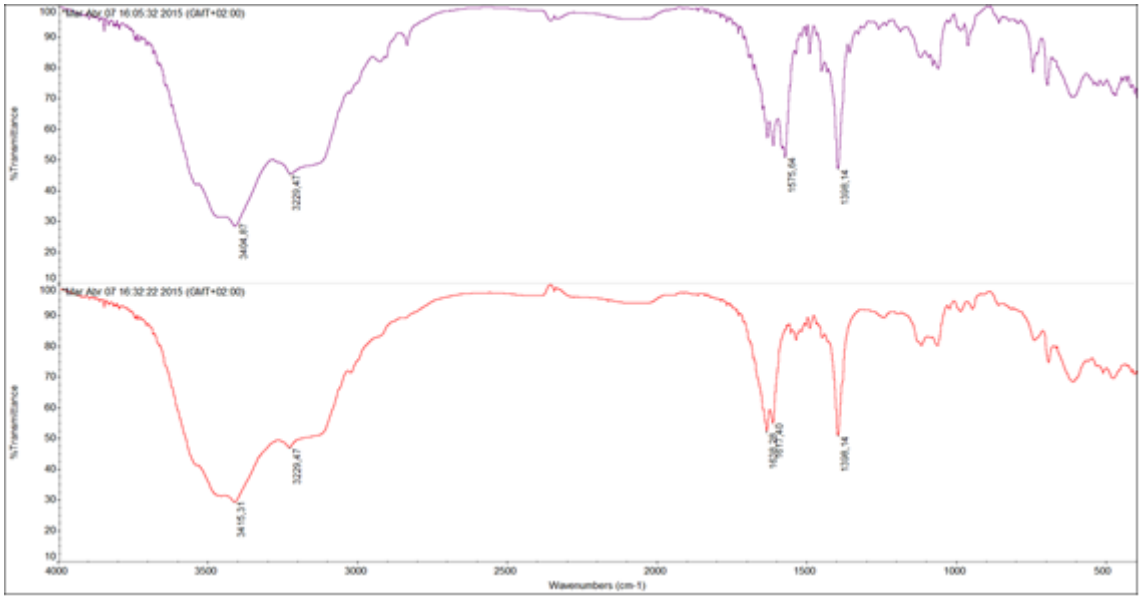

Figure S19. Infrared spectra of **L2** (red line) and Cu**L2** (purple line).

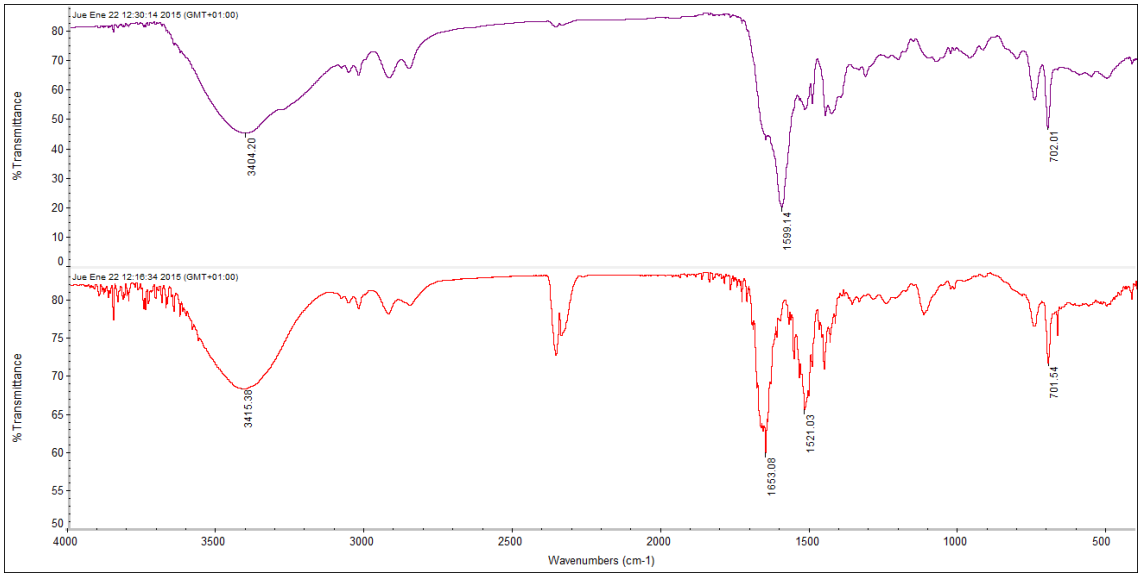

Figure S20. Infrared spectra of **L3** (red line) and Cu_2**L3** (purple line).

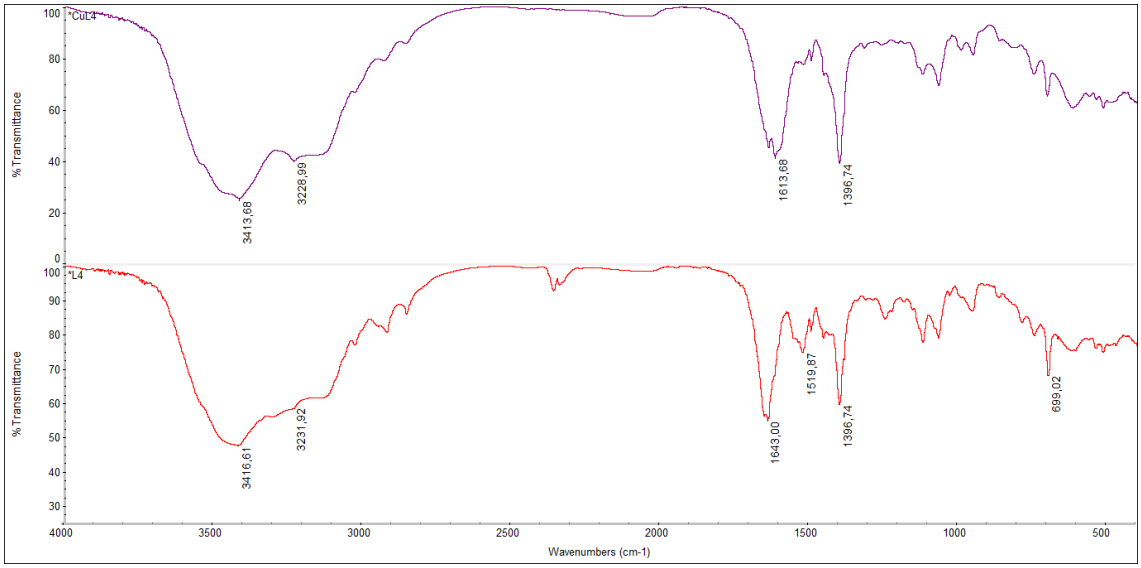

Figure S21. Infrared spectra of **L4** (red line) and Cu_2**L4** (purple line).

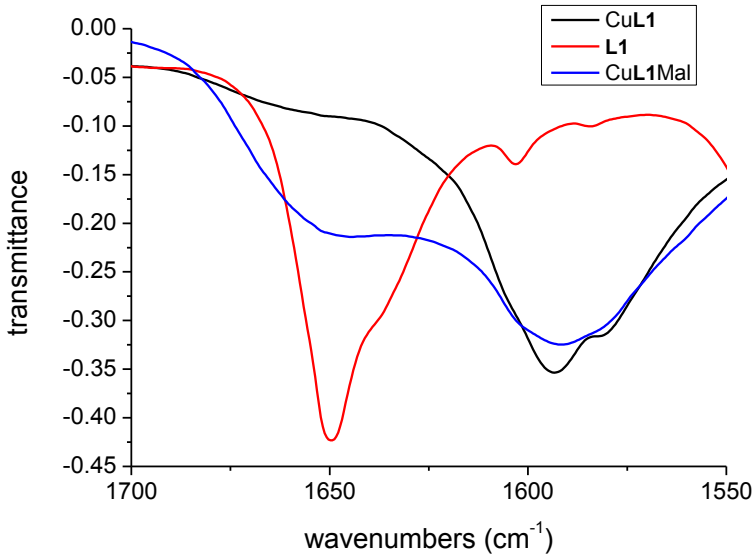

Figure S22. ATR-IR spectra of **L1** (red), Cu**L1** (black) and Cu**L1** plus $(TBA)_2$-L-malate (1:1) (blue).

4. X-rays Crystallographic Analysis

Table S1. Crystal data and structure refinement for **L1** and Cu**L2**.

Compounds	**L1**	Cu**L2**
Empirical formula	C34 H38 N4 O2	C36 H42 Cu N4 O3
Formula weight	534.68	642.27
Temperature	173(2) K	173(2) K
Wavelength	0.71073 Å	0.71073 Å
Crystal system	Triclinic	Orthorhombic
Space group	P 1	P 21 21 21
Unit cell dimensions	a = 9.631(3) Å	a = 10.0943(8) Å
	b = 10.027(3) Å	b = 15.9068(10) Å
	c = 15.551(4) Å	c = 19.5472(13) Å
	α= 86.83(2)°	α= 90°
	β= 87.67(2)°	β= 90°
	γ = 78.27(2)°	γ = 90°
Volume	1467.5(7) Å^3	3138.7(4) Å^3
Z	2	4
Density (calculated)	1.210 Mg/m^3	1.359 Mg/m^3
Absorption coefficient	0.076 mm^{-1}	0.739 mm^{-1}
F(000)	572	1356
Crystal size	0.170 x 0.090 x 0.030 mm^3	0.260 x 0.220 x 0.190 mm^3
Theta range for data collection	3.286 to 25.026°	3.302 to 25.659°
Index ranges	-11<=h<=11	-11<=h<=12
	-11<=k<=11	-19<=k<=16
	-18<=l<=18	-23<=l<=23
Reflections collected	11889	13262
Independent reflections	8265 [R(int) = 0.1832]	5861 [R(int) = 0.0591]
Completeness to theta = 25.000°	99.1 %	99.6 %
Absorption correction	Semi-empirical from equivalents	
Refinement method	Full-matrix least-squares on F^2	
Data / restraints / parameters	8265 / 3 / 721	5861 / 0 / 410
Goodness-of-fit on F^2	1.064	1.002
Final R indices [I>2sigma(I)]	R1 = 0.1479, wR2 = 0.3701	R1 = 0.0365, wR2 = 0.0799
R indices (all data)	R1 = 0.2342, wR2 = 0.4177	R1 = 0.0439, wR2 = 0.0821
Absolute structure parameter	-10.0(10)	-0.025(13)
Extinction coefficient	n/a	n/a
Largest diff. peak and hole	0.544 and -0.661 e.Å^{-3}	0.315 and -0.451 e.Å^{-3}

Table S2. Selected bond distances and angles of X-ray structure of **L1** and Cu**L2**.

L1				**CuL2**			
Distance	**(Å)**	**Angle**	**(º)**	**Distance**	**(Å)**	**Angle**	**(º)**
C2-N1	1.47(2)	N4-C7-C6	109.5(15)	Cu – N2	1.925(3)	N2 – Cu – N3	97.56(14)
C7-N4	1.490(2)	N3-C4-C5	110.2(13)	Cu – N3	1.912(3)	N3 – Cu – N4	83.13(14)
C4-N2	1.50(2)	N1-C2-C3	117.1(15)	Cu – N1	2.037(3)	N2 – Cu – N4	168.15(13)
C5-N3	1.46(2)			Cu – N4	2.049(4)	N1 – Cu – N3	167.89(14)
C6-C3	1.33(0)			N1-C2	1.485(5)	N1 – Cu – N2	82.88(13)
C3-N2	1.34(2)			N2-C3	1.319(6)	N1 – Cu – N4	98.94(13)
C6-O2	1.30(2)			N3-C7	1.327(5)		
C2-O1	1.29(8)			N4-C8	1.486(5)		

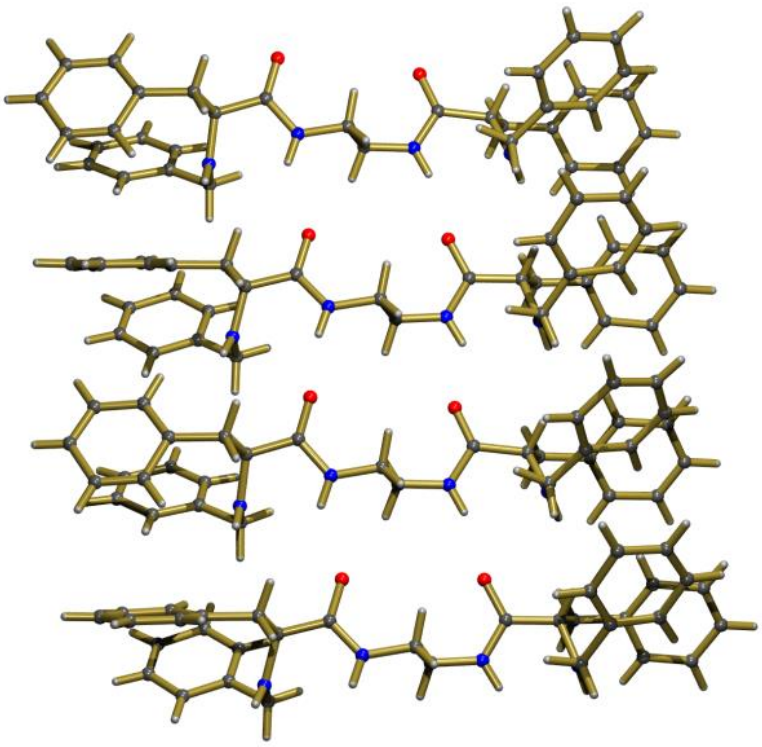

Figure S23. Parallel disposition of the molecules of **L1** in the crystal structure.

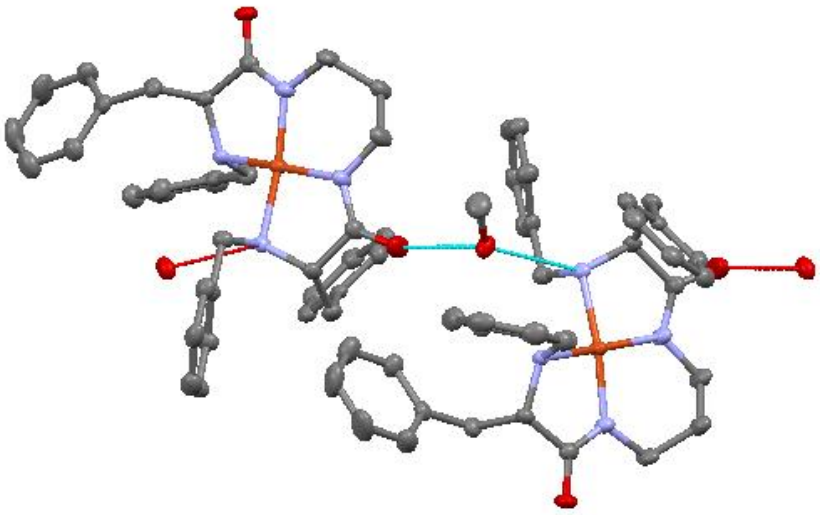

Figure S24. Hydrogen bonds established between the methanol crystallized molecule and two molecules of Cu**L2**.

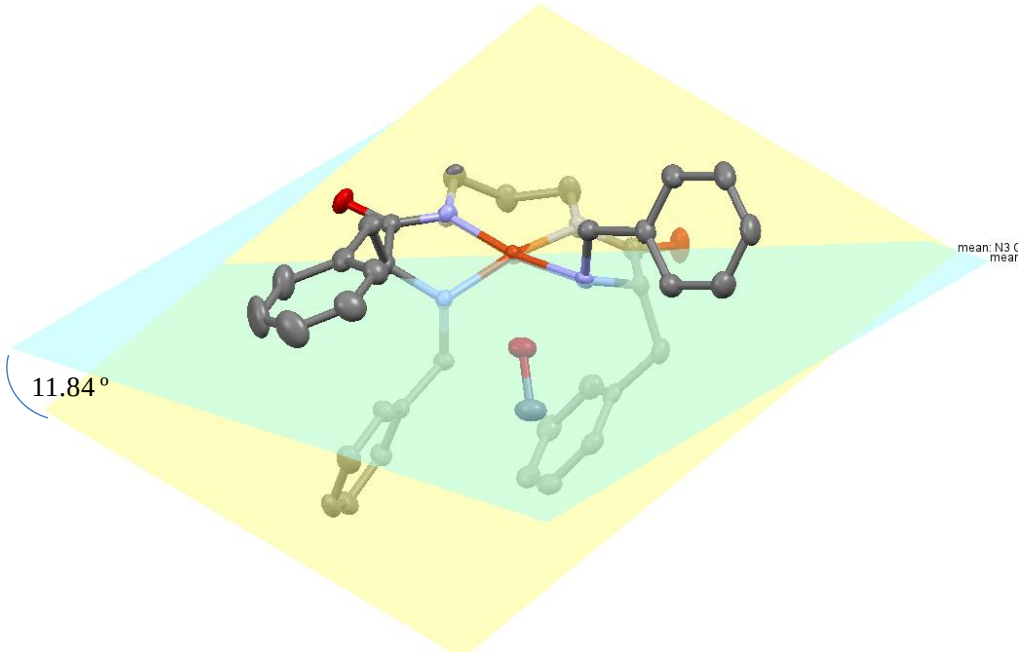

Figure S25. Torsion angle displayed by the Cu-complex coordination.

5. EPR spectra

Table S3. Best fit EPR spectroscopic parameters of Cu complexes in solid solution (MeOH, 103 K)

	$A_{\parallel}$	$A_{\perp}$	A_N	$g_{\parallel}$	$g_{\perp}$	$g_{\parallel}/A_{\parallel}$	type
$CuAsp_2$	167.5	17.6	11.3	2.26112	2.04634	127.9	CuN_2O_2
$CuMal_2$	122.2	13.4	---	2.38329	2.07146	175.2	CuO_4

	$A_{\parallel}$	$A_{\perp}$	A_N	$g_{\parallel}$	$g_{\perp}$	$g_{\parallel}/A_{\parallel}$	type
CuL1	199.5	23.6	14.7	2.18220	2.04135	107.4	CuN_4
CuL2	200.8	21.0	15.67	2.18521	2.04139	108.8	CuN_4
Cu_2L3	190.4	23.2	14.8	2.18843	2.04365	112.5	CuN_4
Cu_2L4	197.5	24.8	14.7	2.18465	2.04048	108.5	CuN_4

CuL1 plus different anions

	$A_{\parallel}$	$A_{\perp}$	A_N	$g_{\parallel}$	$g_{\perp}$	$g_{\parallel}/A_{\parallel}$	type
CuL1	199.5	23.6	14.7	2.18220	2.04135	107.4	CuN_4
CuL1 + Asp	167.6	18.9	12.4	2.26265	2.04751	127.8	CuN_2O_2
CuL1 + Mal	168.6	24.8	12.8	2.23767	2.04773	127.0	CuN_2O_2
minor component	169.4	18.2	12.8	2.18311	2.04082	126.4	CuN_2O_2

Cu_2L3 plus different anions

Cu_2L3	190.4	23.2	14.8	2.18843	2.04365	112.5	CuN4
Cu_2L3 + Suc	191.4	23.2	14.8	2.18625	2.04858	111.9	CuN4
Cu_2L3 + Mal	162.8	25.6	14.8	2.24220	2.04873	131.6	CuN_2O_2
Cu_2L3 + Asp	168.2	17.6	12.3	2.26092	2.04923	127.4	CuN_2O_2

Cu_2L4 plus different anions

Cu_2L4	197.5	24.8	14.7	2.18465	2.040480	108.5	CuN_4
Cu_2L4 + Mal	162.8	25.6	14.8	2.24220	2.04673	131.6	CuN_2O_2
Cu_2L4 + Asp	169.2	18.2	11.7	2.25840	2.04729	126.6	CuN_2O_2

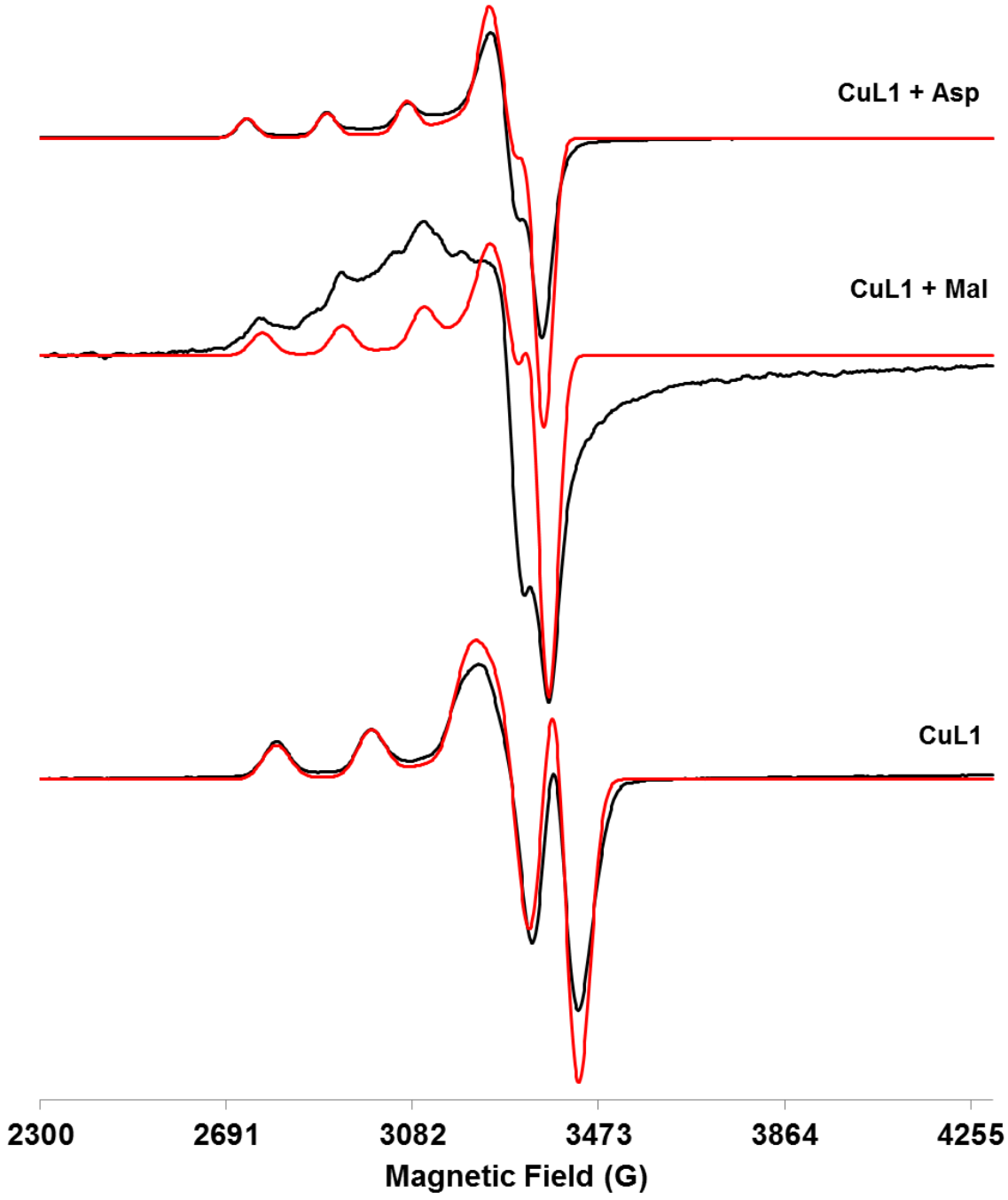

Figure S26. X-band EPR spectra of a frozen methanol solution (103 K) of Cu**L1** alone and in the presence of different dicarboxylate anions (black: experimental; red: simulated).

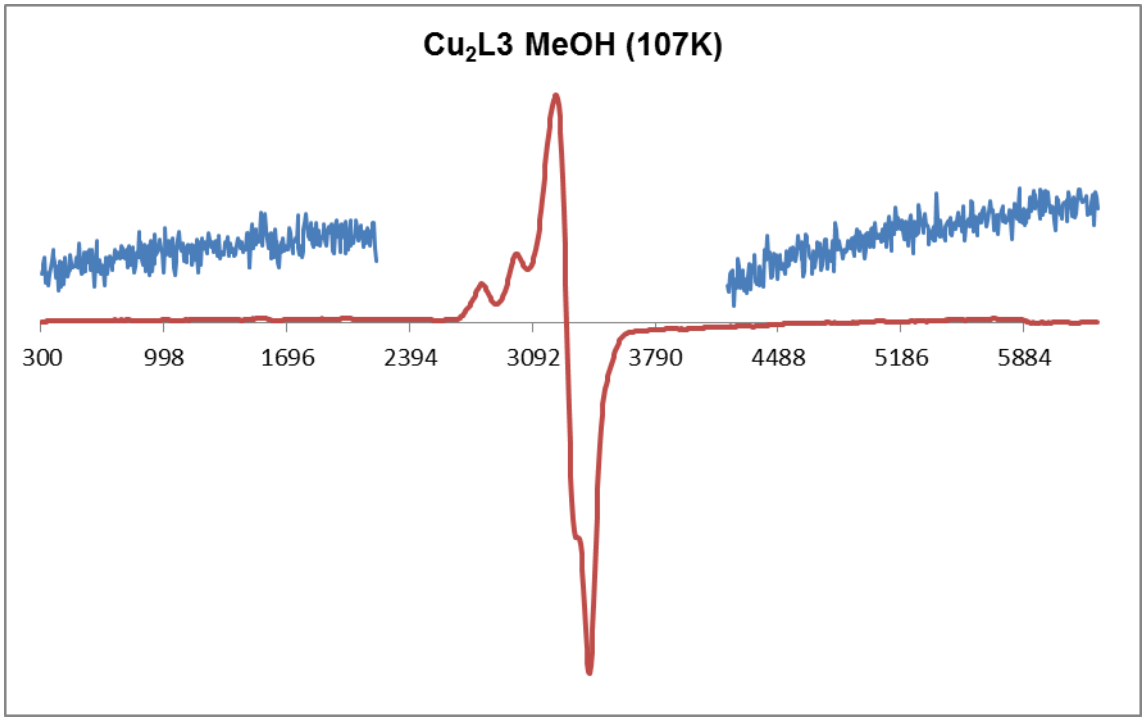

Fig. S27. In red: X-band EPR spectra of a frozen methanol solution (107 K) of Cu_2**L3** complex (field scan range from 300 to 6300 G). In blue: 10x magnification of selected regions of the spectrum.

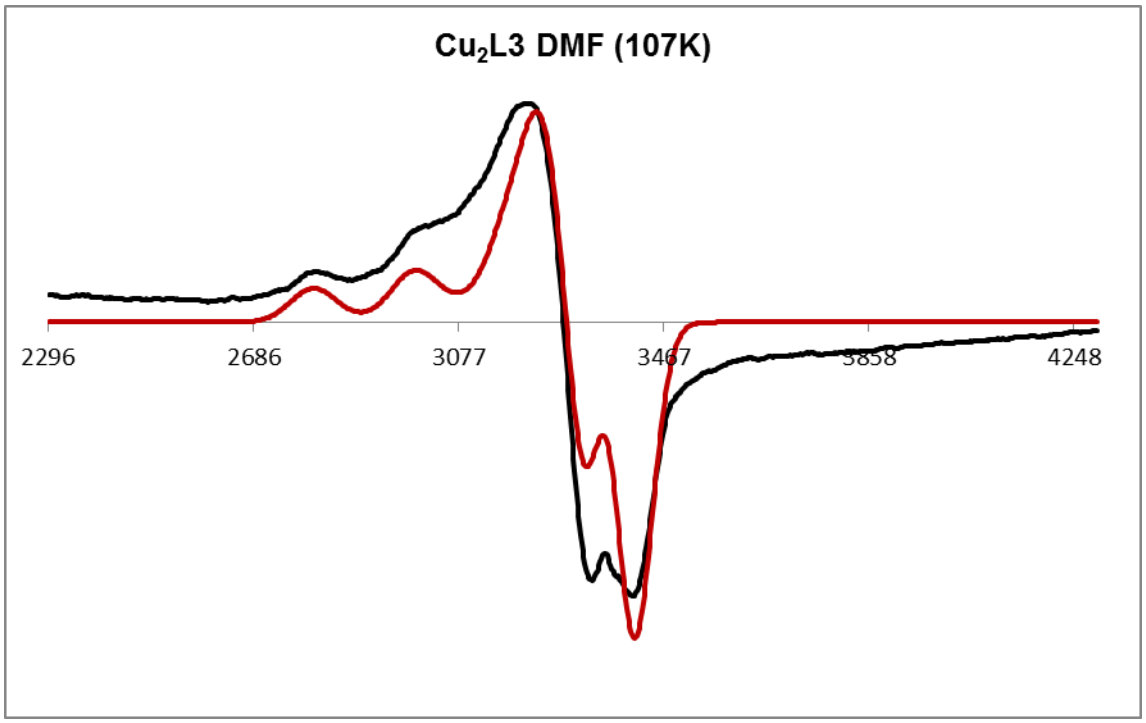

Fig. S28. X-band EPR spectrum of a frozen DMF solution (107 K) of Cu_2**L3** complex (black: experimental; red: simulated). Spectral parameters: ($A_{\parallel}$ = 194.3 G; $A_{\perp}$ = 22.6 G; A_N = 14.8 G; $g_{\parallel}$ =2.18395; $g_{\perp}$ = 2.04397).

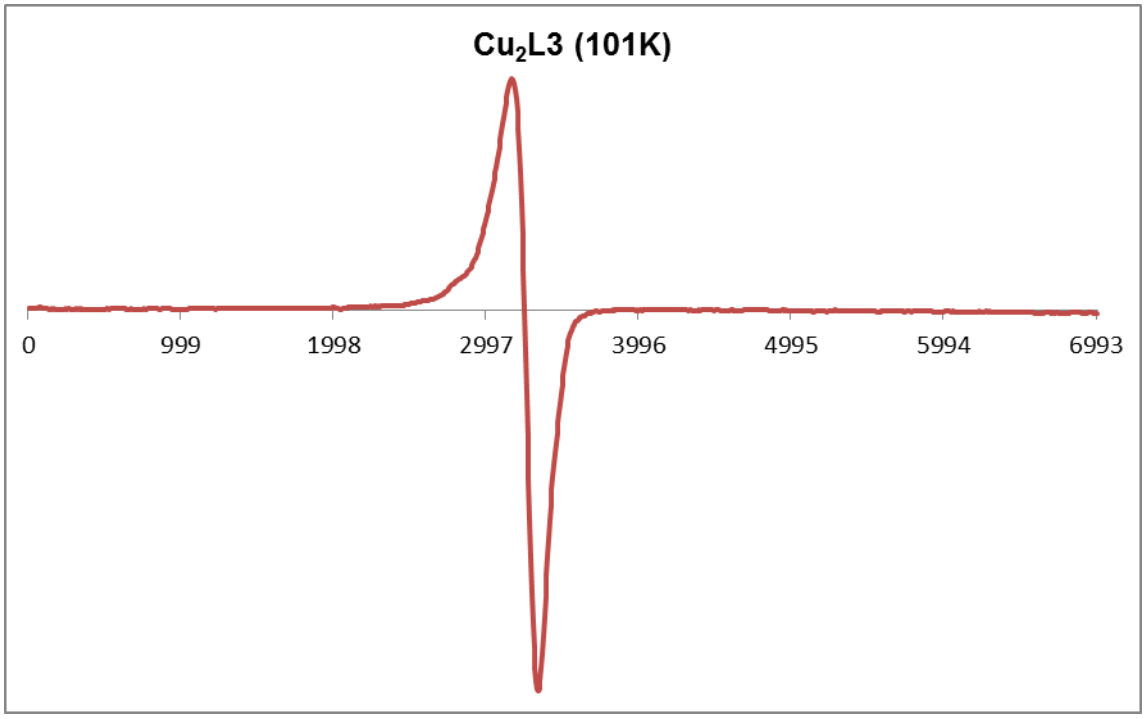

Fig. S29. X-band EPR spectrum (101 K) of Cu_2**L3** complex in solid state (field scan range from 0 to 7000 G).

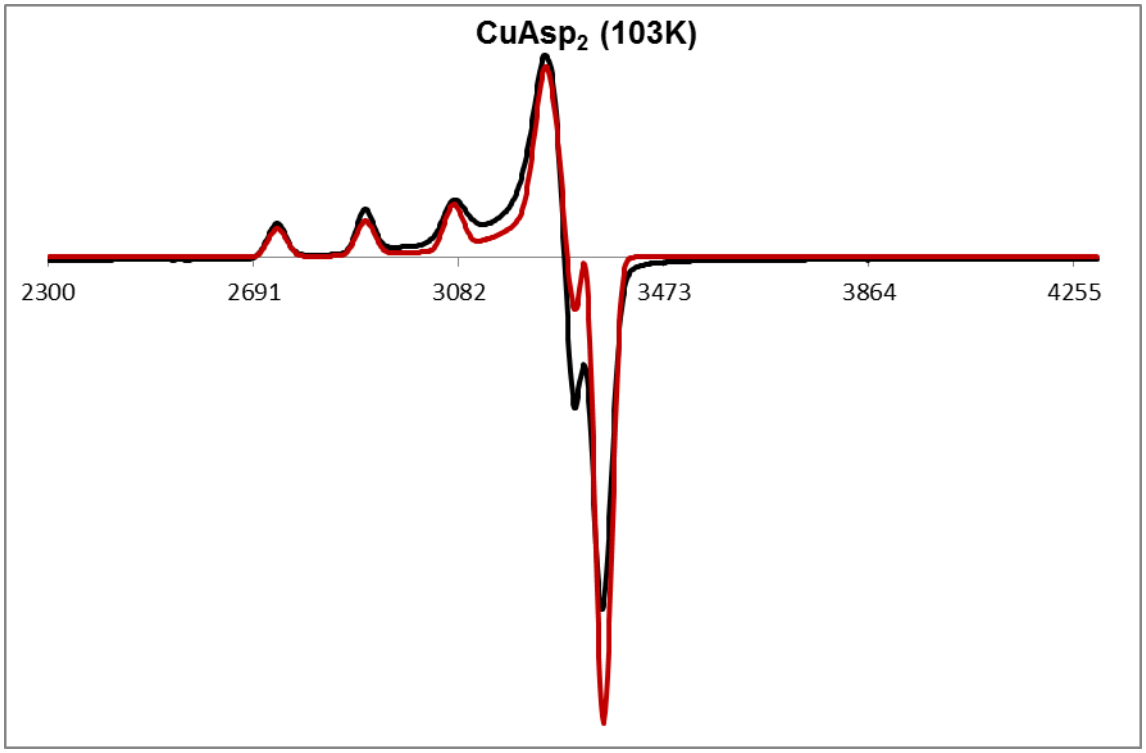

Fig. S30. X-band EPR spectrum of a frozen methanol solution (103 K) of $CuAsp_2$ (black: experimental; red: simulated).

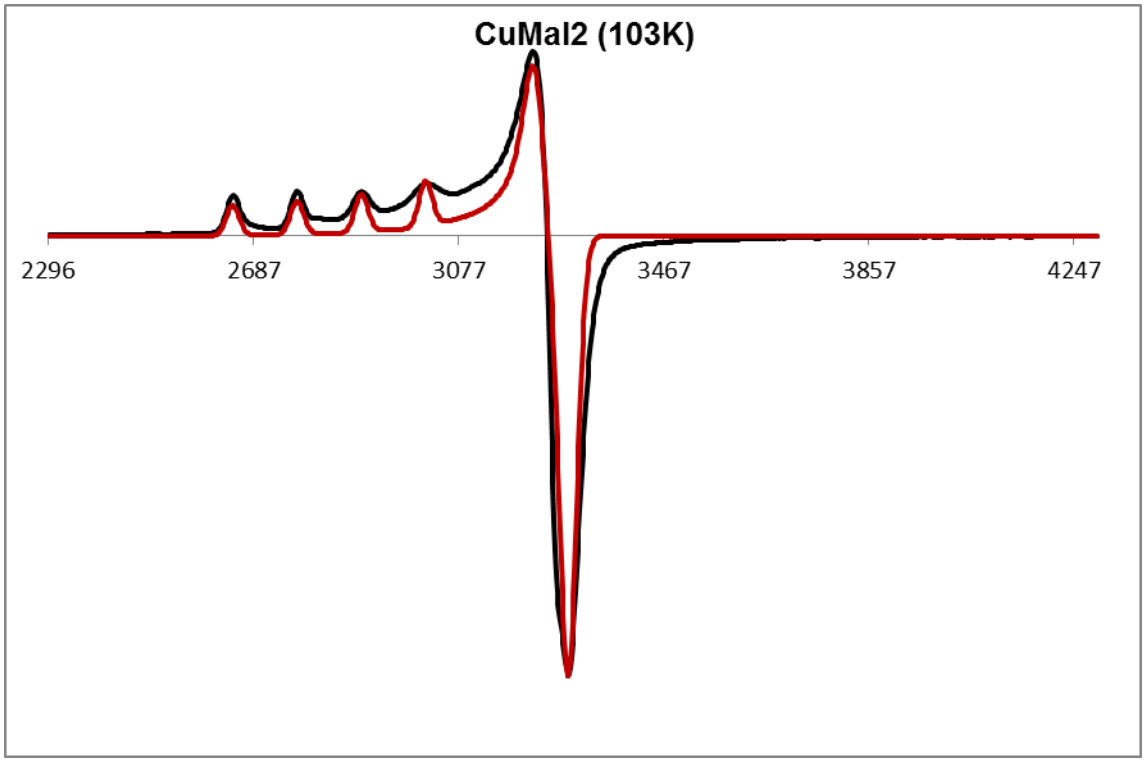

Fig. S31. X-band EPR spectrum of a frozen methanol solution (103 K) of $CuMal_2$. (black: experimental; red: simulated).

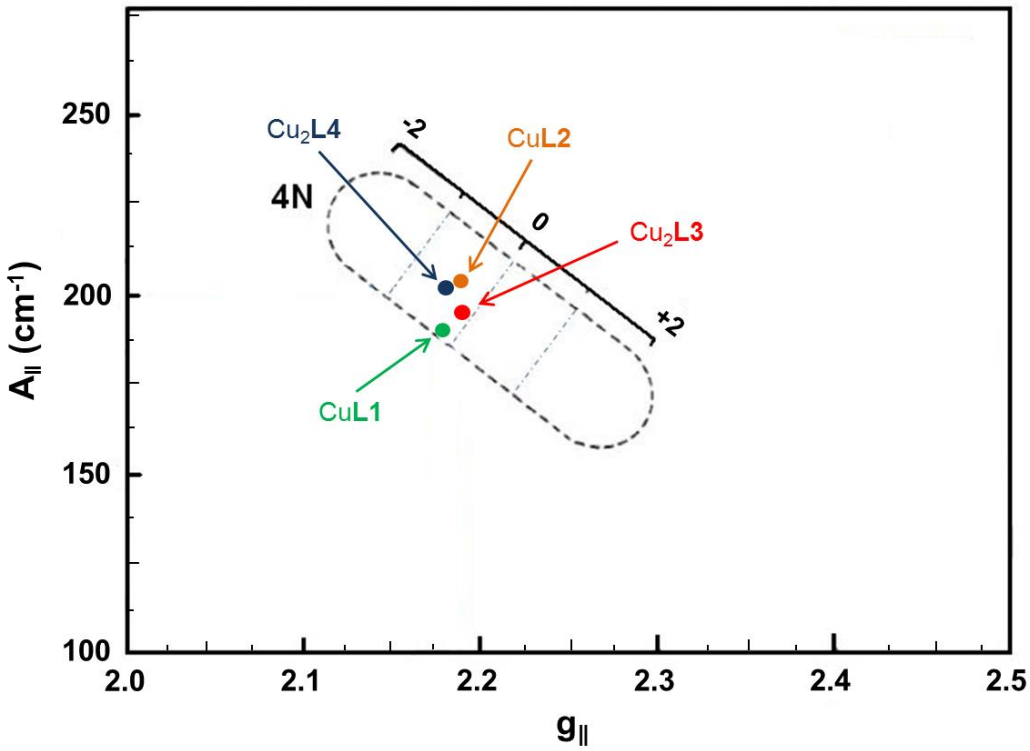

Figure S32. Peisach and Blumberg plot of Cu**L1**, Cu**L2**, Cu_2**L3** and Cu_2**L4**.

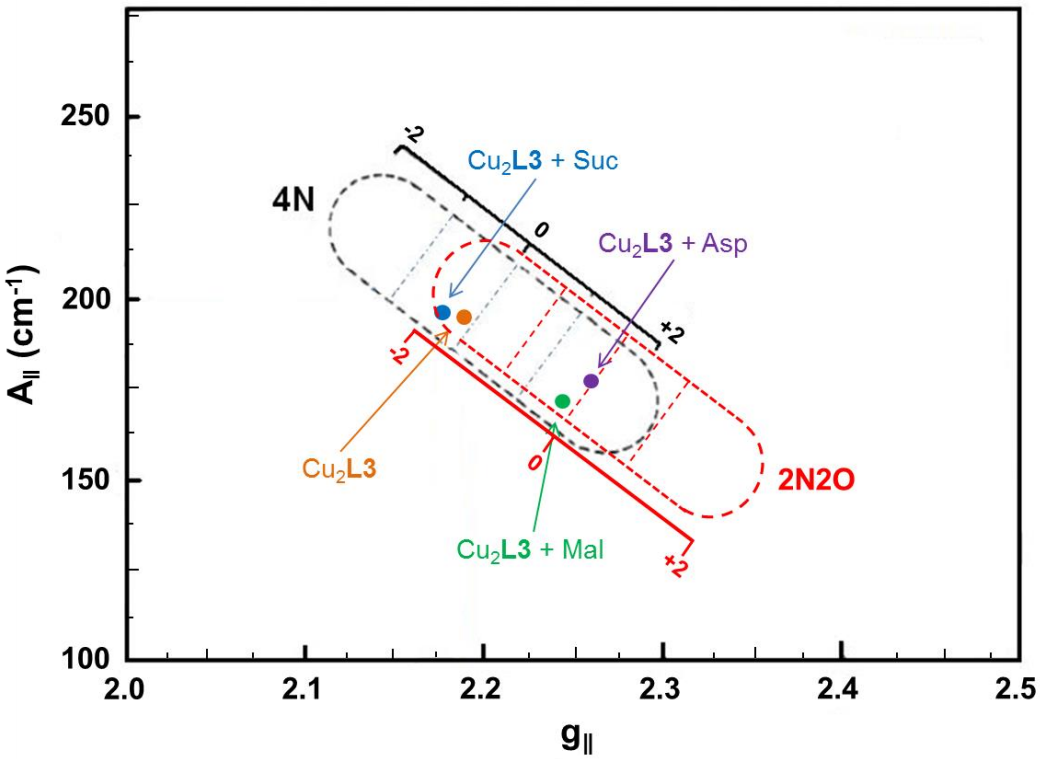

Figure S33. Peisach and Blumberg plot of Cu_2**L3**, Cu_2**L3** + $(TBA)_2$-Succinate, Cu_2**L3** + $(TBA)_2$-Malate and Cu_2**L3** + $(TBA)_2$-Aspartate.

6. UV-vis titrations

Cu_2**L3** *vs.* dicarboxylates

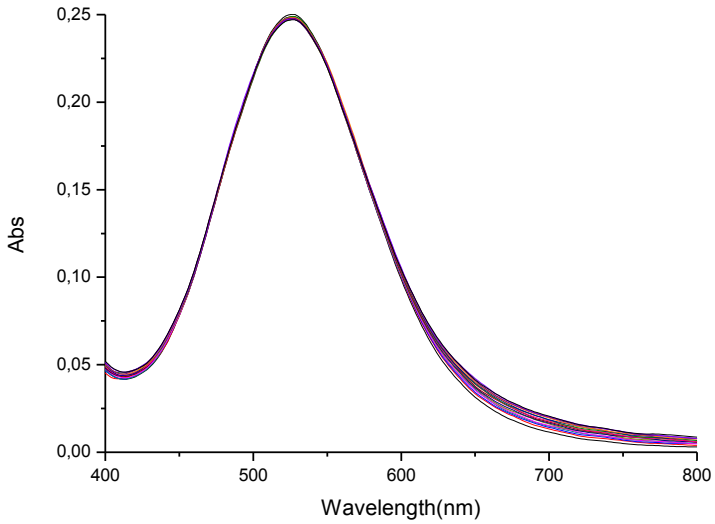

Figure S34. UV-vis spectra of Cu_2**L3** ($7.0 \cdot 10^{-4}$ M, MeOH) in presence of increasing amounts of $(TBA)_2$-Succinate (0-$2.8 \cdot 10^{-3}$ M; 0-4 eqs.).

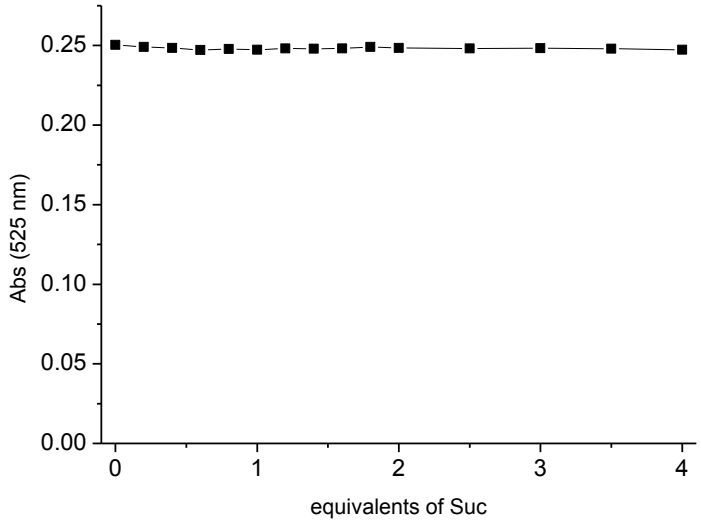

Figure S35. Changes in the absorbance at 525 nm of Cu_2**L3** upon addition of $(TBA)_2$-Succinate.

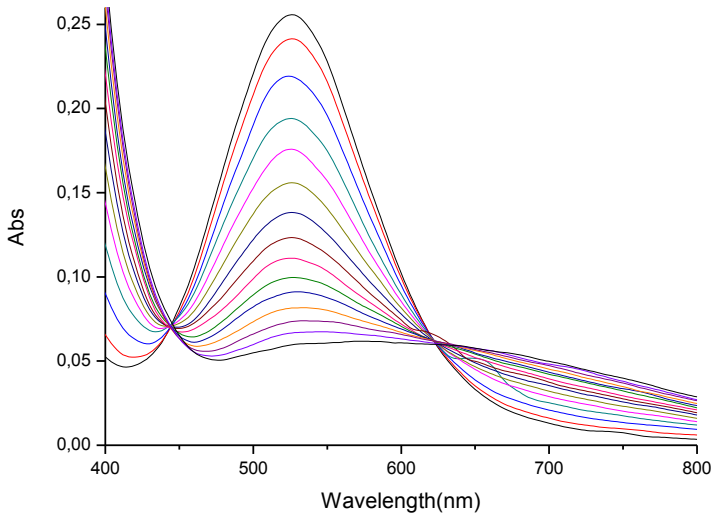

Figure S36. UV-vis spectra of Cu_2**L3** ($7.0 \cdot 10^{-4}$ M, MeOH) in presence of increasing amounts of $(TBA)_2$-L-malate ($0\text{-}2.8 \cdot 10^{-3}$ M; 0-4 eqs.).

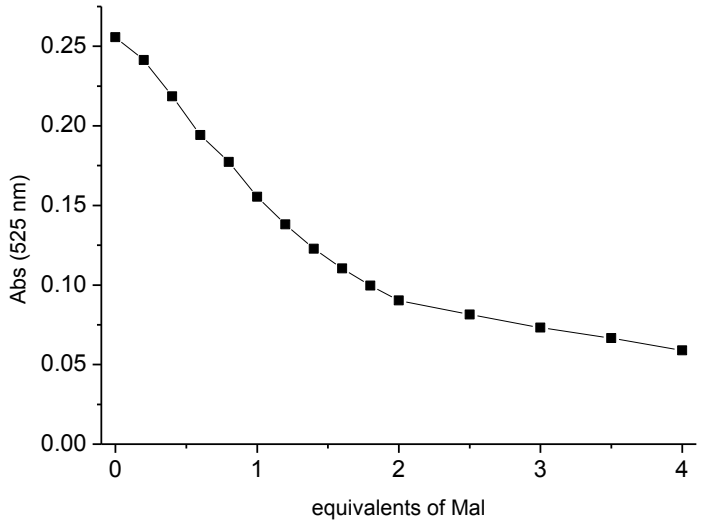

Figure S37. Changes in the absorbance at 525 nm of Cu_2**L3** upon addition of $(TBA)_2$-Malate.

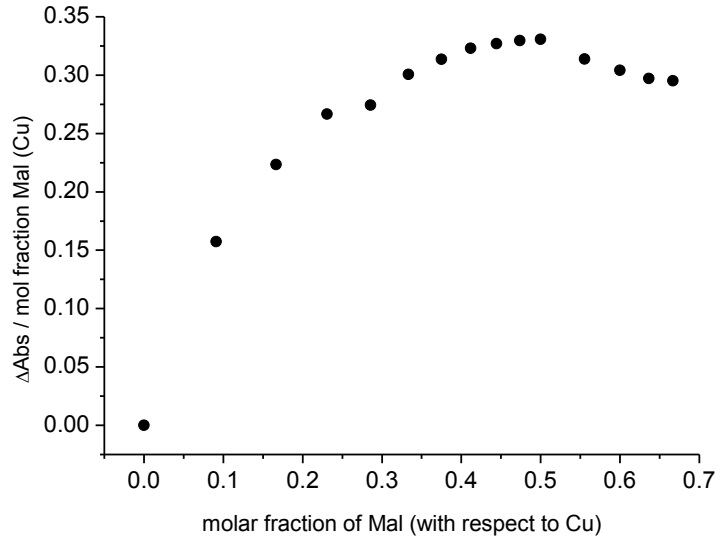

Figure S38. Job plot for the Cu_2**L3** - $(TBA)_2$-Malate system.

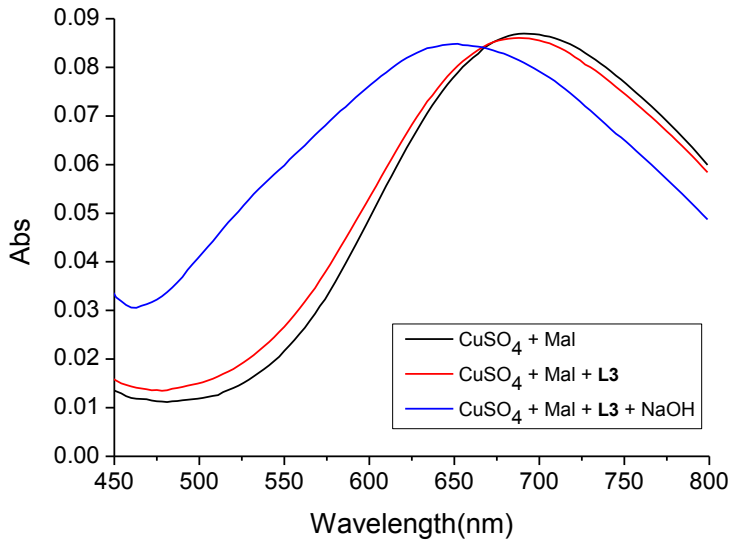

Figure S39. UV-vis spectra comparison (MeOH). Black: $CuSO_4$ [$2 \cdot 10^{-3}$ M] + 2.0 eqs. of $(TBA)_2$-Malate; Red: after the addition of 0.5 eqs. of **L3**; Blue: after the further addition of 2.0 eqs. of NaOH.

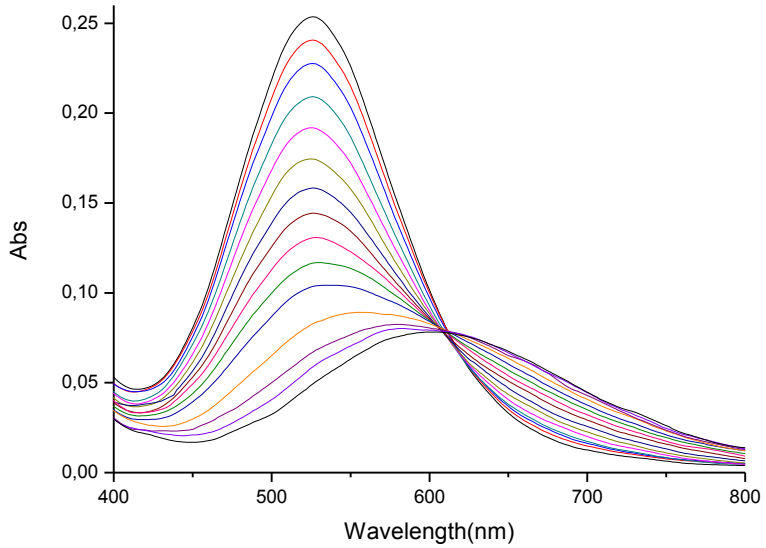

Figure S40. UV-vis spectra of Cu_2**L3** ($7.0 \cdot 10^{-4}$ M, MeOH) in presence of increasing amounts of $(TBA)_2$-L-glutamate ($0\text{-}2.8 \cdot 10^{-3}$ M; 0-4 eqs.).

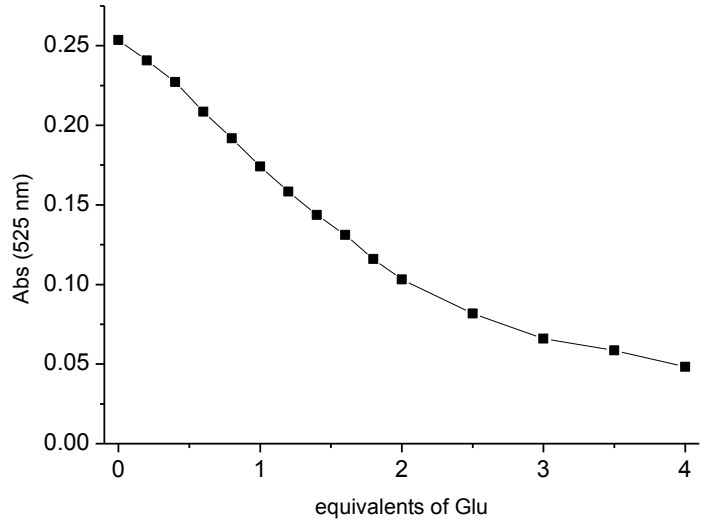

Figure S41. Changes in the absorbance at 525 nm of Cu_2**L3** upon addition of $(TBA)_2$-Glutamate.

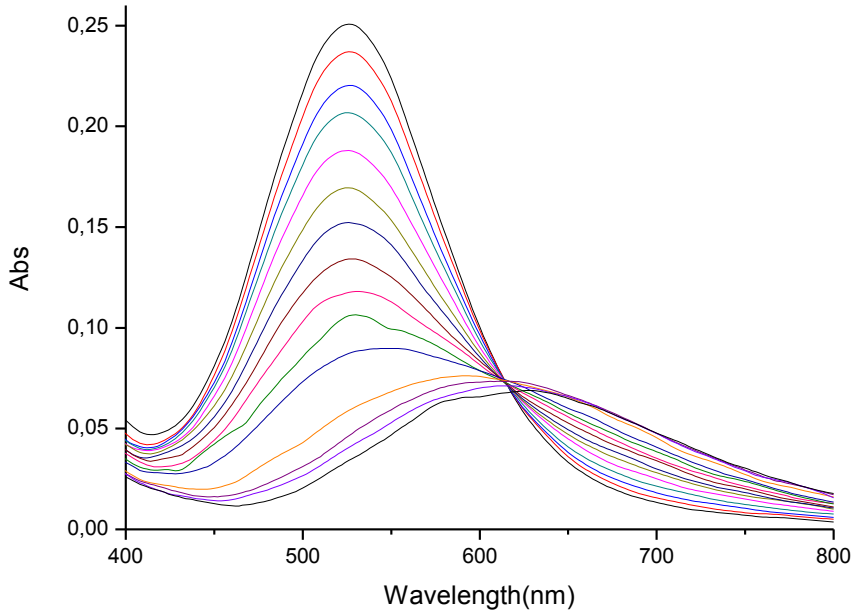

Figure S42. UV-vis spectra of Cu_2**L3** ($7.0 \cdot 10^{-4}$ M, MeOH) in presence of increasing amounts of $(TBA)_2$-L-aspartate ($0\text{-}2.8 \cdot 10^{-3}$ M; 0-4 eqs.).

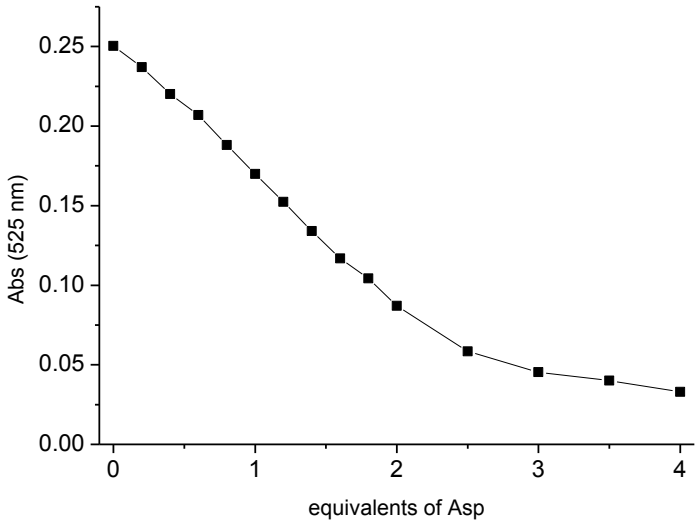

Figure S43. Changes in the absorbance at 525 nm of Cu_2**L3** upon addition of $(TBA)_2$-Aspartate.

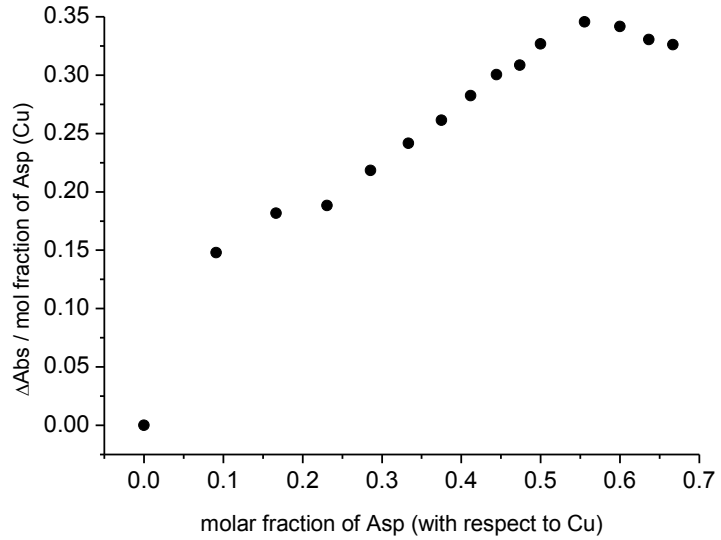

Figure S44. Job plot for the Cu_2**L3** - $(TBA)_2$-Aspartate system.

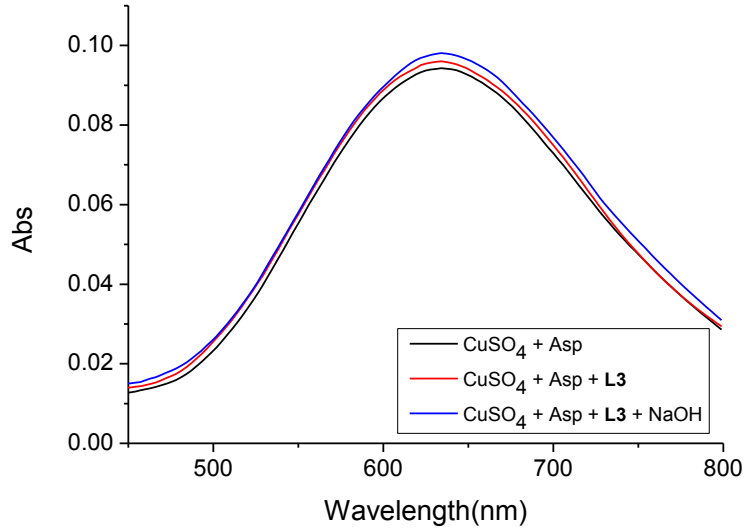

Figure S45. UV-vis spectra comparison (MeOH). Black: $CuSO_4$ [$2 \cdot 10^{-3}$ M] + 2.0 eqs. of $(TBA)_2$-Aspartate; Red: after the addition of 0.5 eqs. of **L3**; Blue: after the further addition of 2.0 eqs. of NaOH.

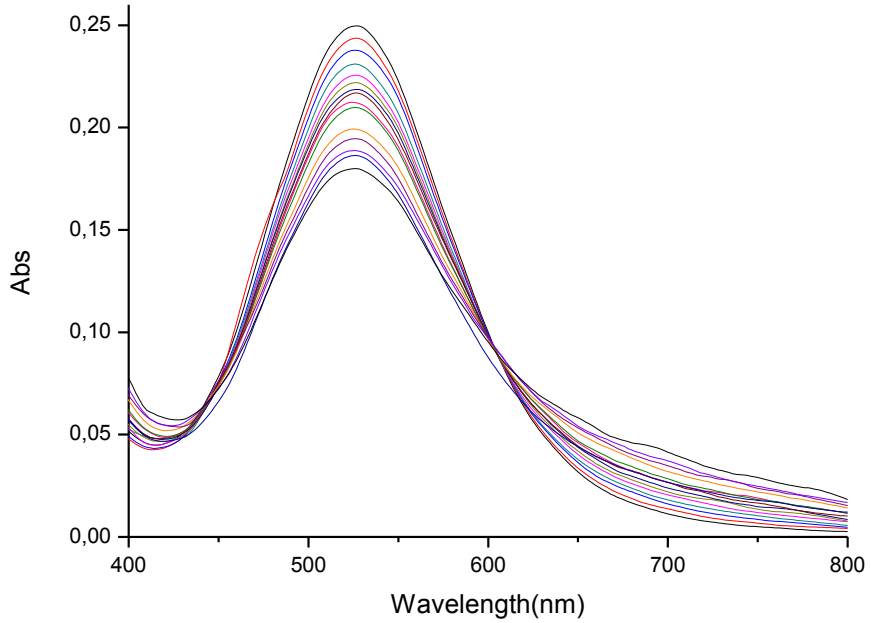

Figure S46. UV-vis spectra of Cu_2**L3** ($7.0 \cdot 10^{-4}$ M, MeOH) in presence of increasing amounts of $(TBA)_2$-*N*-acetyl-L-aspartate (0-$2.8 \cdot 10^{-3}$ M; 0-4 eqs.).

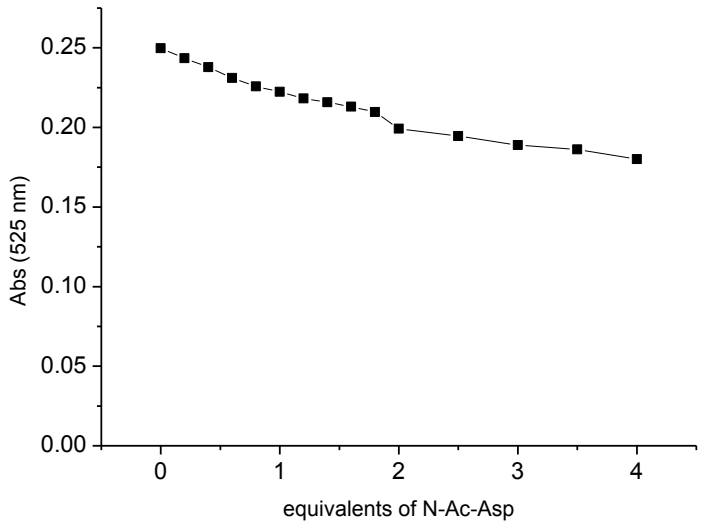

Figure S47. Changes in the absorbance at 525 nm of Cu_2**L3** upon addition of $(TBA)_2$-*N*-Ac-Aspartate.

Cu_2**L4** *vs.* dicarboxylates

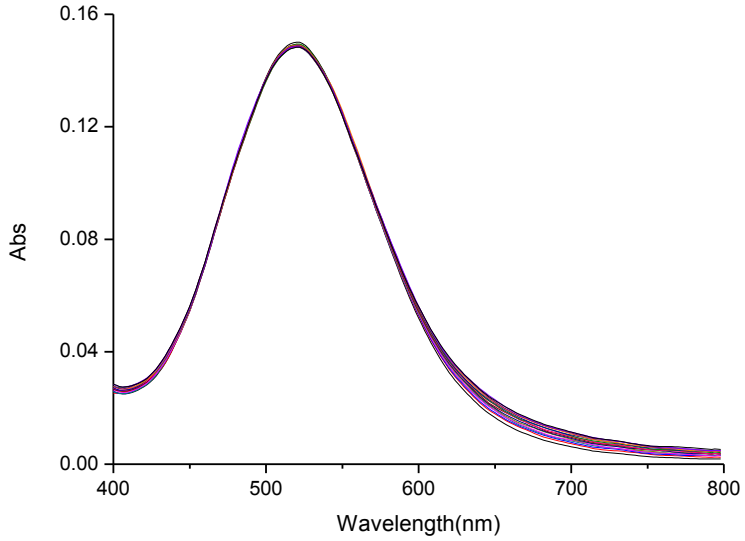

Figure S48. UV-vis spectra of Cu_2**L4** ($5.0 \cdot 10^{-4}$ M, MeOH) in presence of increasing amounts of $(TBA)_2$-Succinate ($0\text{-}2.0 \cdot 10^{-3}$ M; 0-3 eqs.).

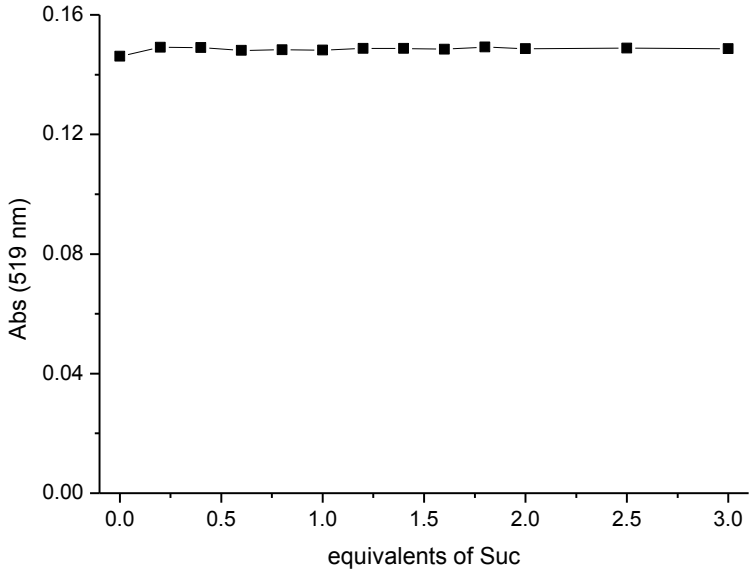

Figure S49. Changes in the absorbance at 519 nm of Cu_2**L4** upon addition of $(TBA)_2$-Succinate.

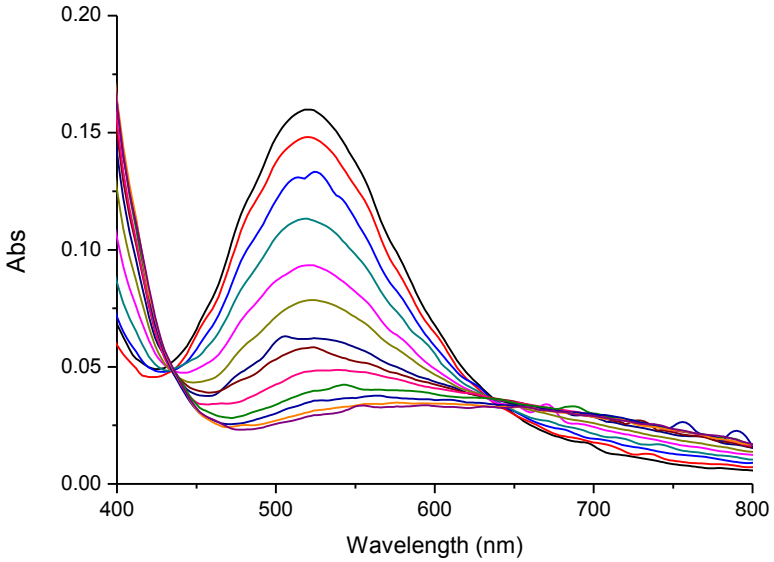

Figure S50. UV-vis spectra of Cu_2**L4** ($5.0 \cdot 10^{-4}$ M, MeOH) in presence of increasing amounts of $(TBA)_2$-Malate ($0\text{-}2.0 \cdot 10^{-3}$ M; 0-4 eqs.).

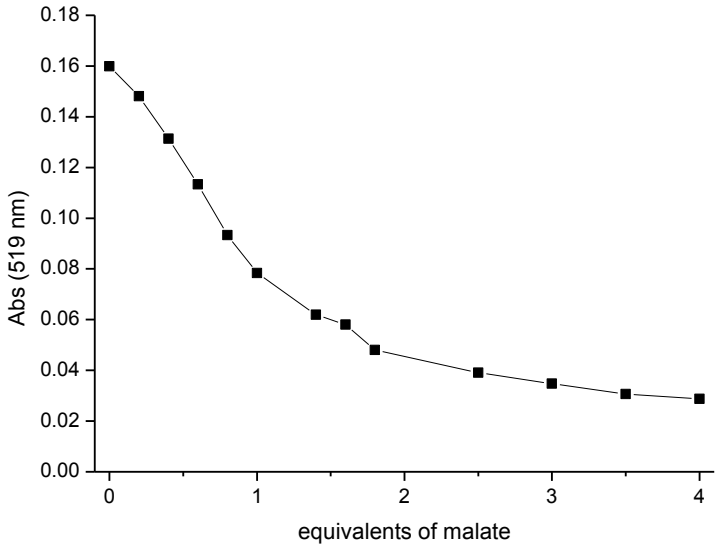

Figure S51. Changes in the absorbance at 519 nm of Cu_2**L4** upon addition of $(TBA)_2$-Malate.

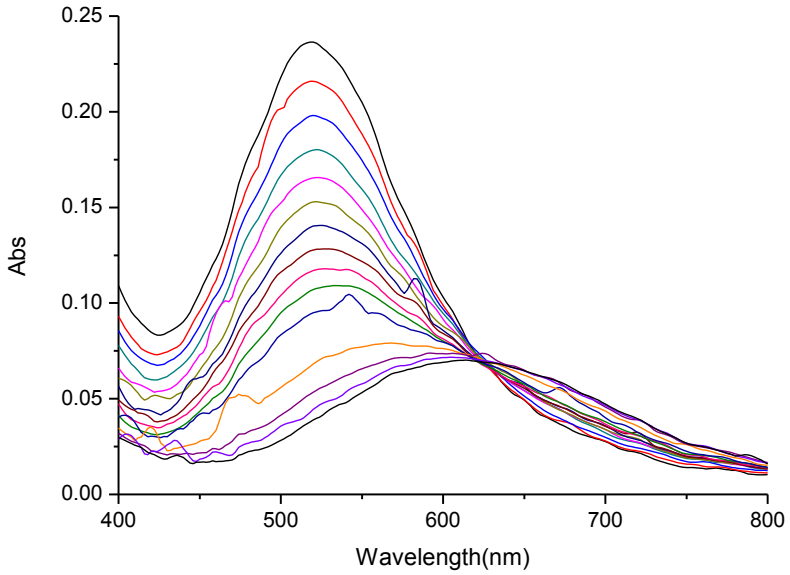

Figure S52. UV-vis spectra of Cu_2**L4** ($7.5.0 \cdot 10^{-4}$ M, MeOH) in presence of increasing amounts of $(TBA)_2$-Aspartate ($0\text{-}3.0 \cdot 10^{-3}$ M; 0-4 eqs.).

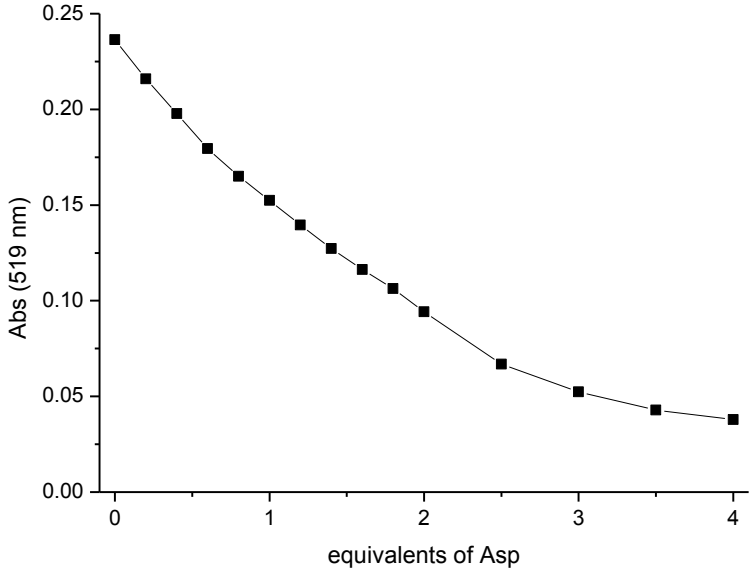

Figure S53. Changes in the absorbance at 519 nm of Cu_2**L4** upon addition of $(TBA)_2$-Aspartate.

Cu**L1** *vs.* dicarboxylates

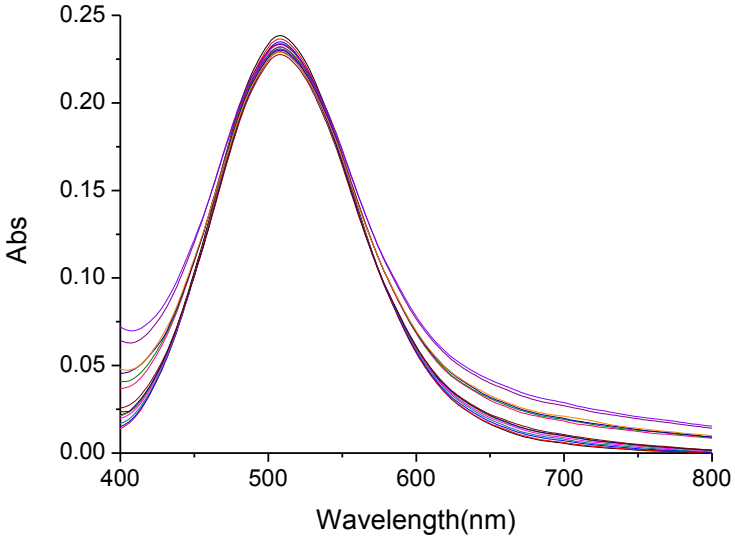

Figure S54. UV-vis spectra of Cu**L1** ($1.0 \cdot 10^{-3}$ M, MeOH) in presence of increasing amounts of $(TBA)_2$-Succinate ($0\text{-}3.0 \cdot 10^{-3}$ M; 0-3 eqs.).

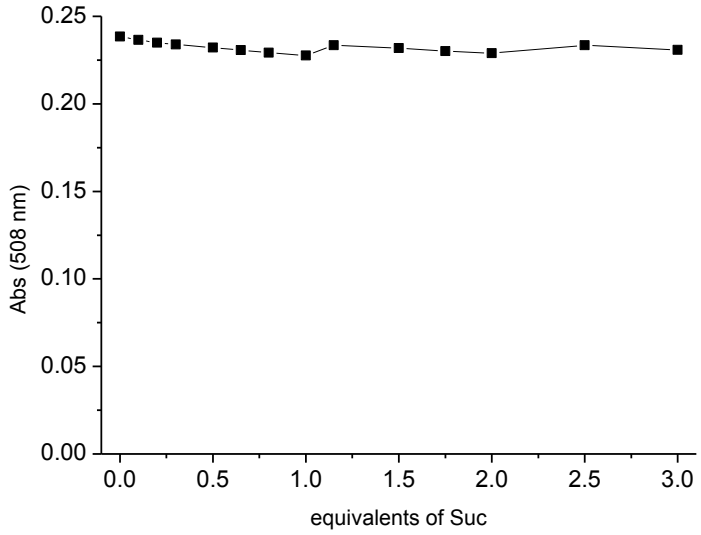

Figure S55. Changes in the absorbance at 508 nm of Cu**L1** upon addition of $(TBA)_2$-Succinate.

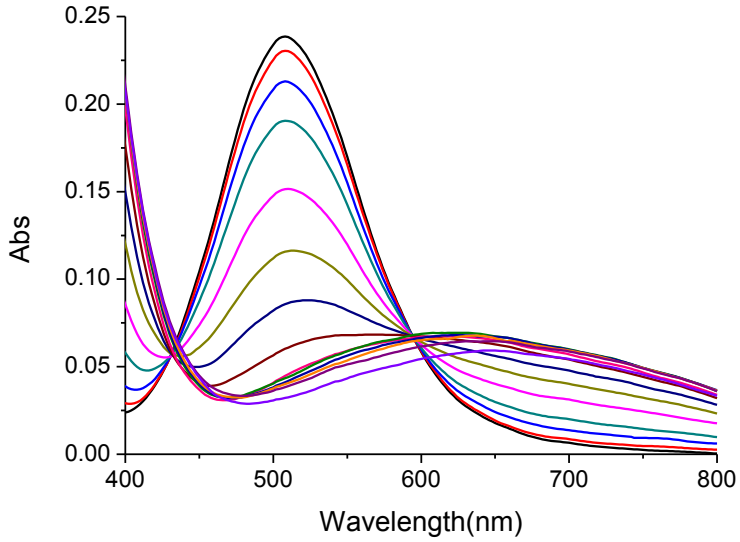

Figure S56. UV-vis spectra of Cu**L1** ($1.0 \cdot 10^{-3}$ M, MeOH) in presence of increasing amounts of $(TBA)_2$-Malate ($0\text{-}3.0 \cdot 10^{-3}$ M; 0-3 eqs.).

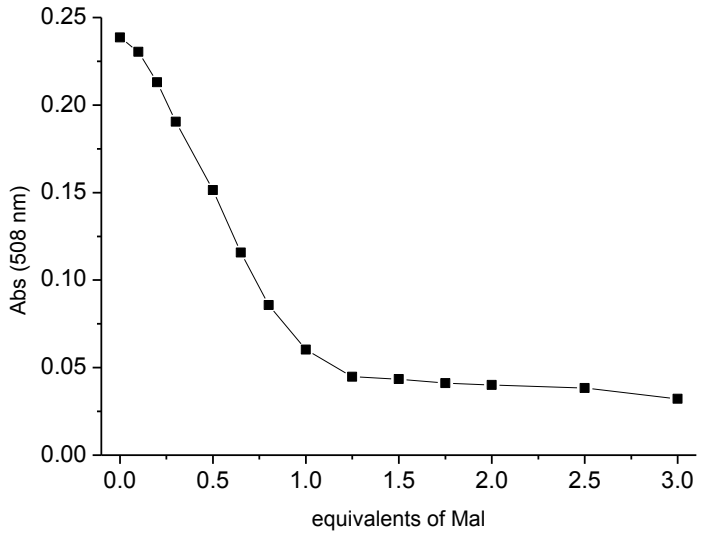

Figure S57. Changes in the absorbance at 508 nm of Cu**L1** upon addition of $(TBA)_2$-Malate.

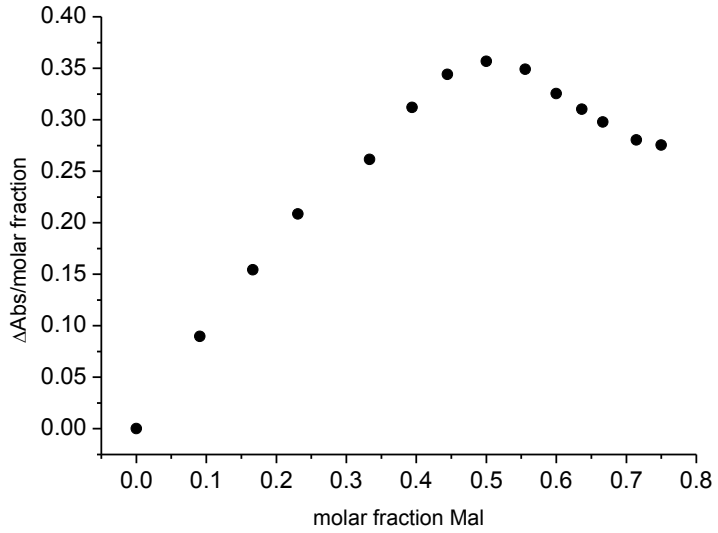

Figure S58. Job plot for the Cu**L1** - $(TBA)_2$-Malate system.

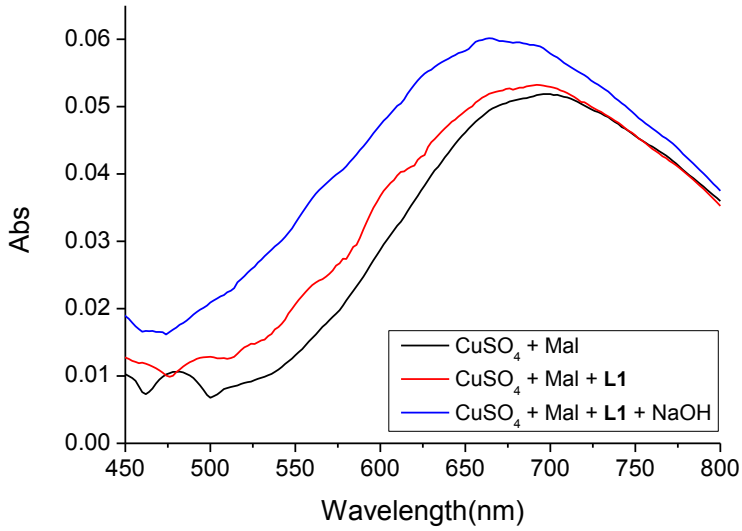

Figure S59. UV-vis spectra comparison (MeOH). Black: $CuSO_4$ [$1 \cdot 10^{-3}$ M] + 2.0 eqs. of $(TBA)_2$-Malate; Red: after the addition of 1.0 eq. of **L1**; Blue: after the further addition of 2.0 eqs. of NaOH.

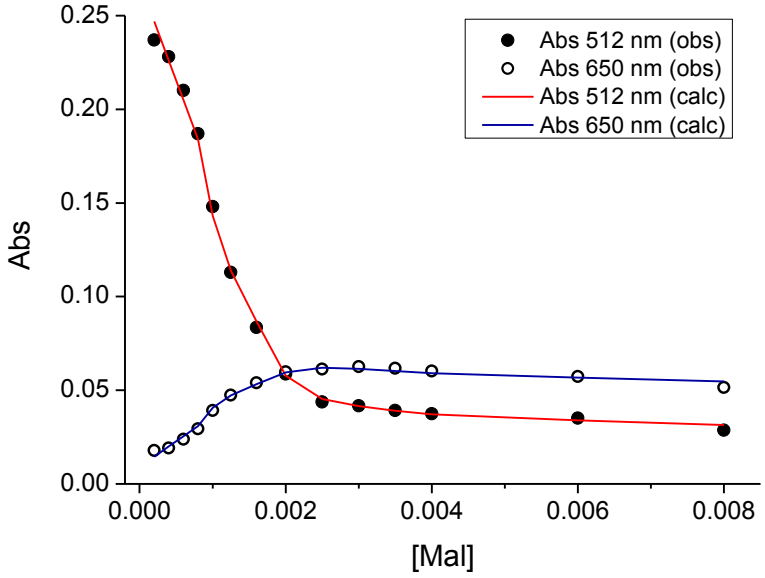

Figure S60. Absorbance values at 512 nm and 650 nm of Cu**L1** upon titration with $(TBA)_2$-L-Malate (symbols: experimental data; lines: fitted data).

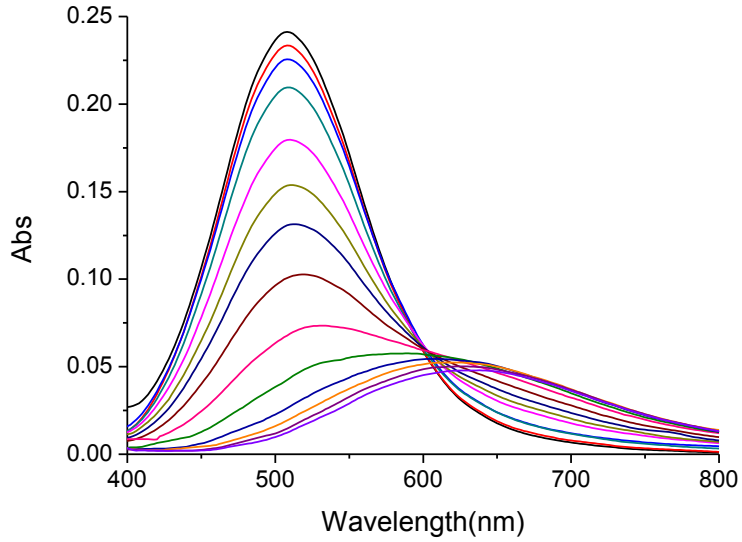

Figure S61. UV-vis spectra of Cu**L1** ($1.0 \cdot 10^{-3}$ M, MeOH) in presence of increasing amounts of $(TBA)_2$-Aspartate ($0\text{-}3.0 \cdot 10^{-3}$ M; 0-3 eqs.).

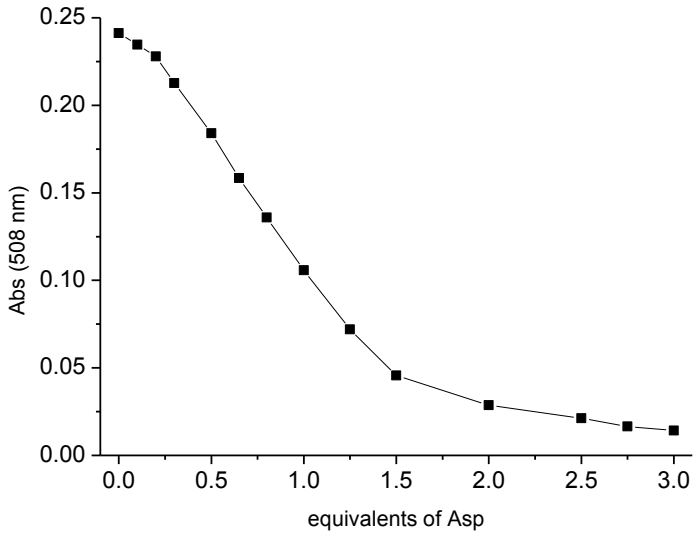

Figure S62. Changes in the absorbance at 508 nm of Cu**L1** upon addition of $(TBA)_2$-Aspartate.

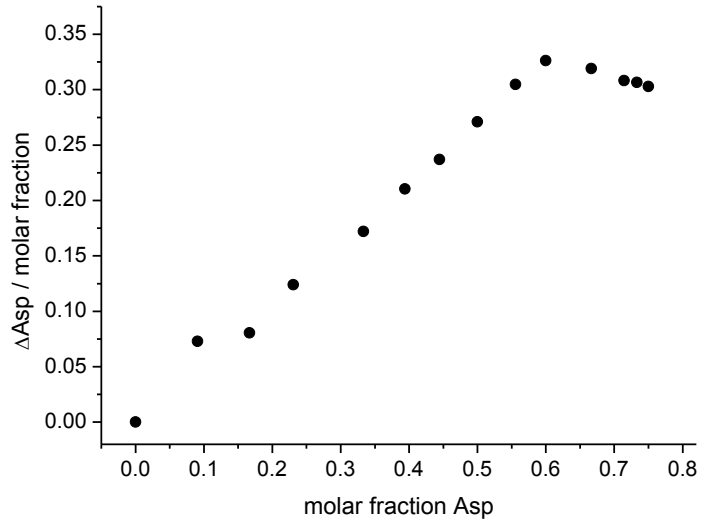

Figure S63. Job plot for the Cu**L1** - $(TBA)_2$-Aspartate system.

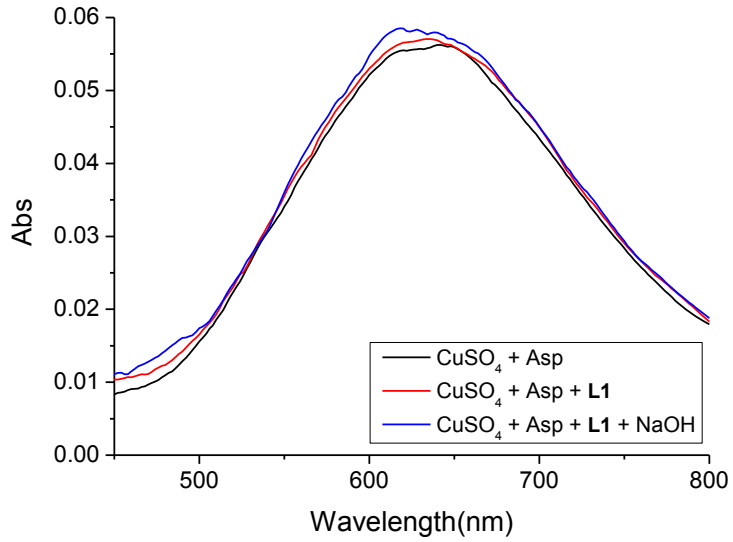

Figure S64. UV-vis spectra comparison (MeOH). Black: $CuSO_4$ [$1 \cdot 10^{-3}$ M] + 2.0 eqs. of $(TBA)_2$-Aspartate; Red: after the addition of 1.0 eq. of **L1**; Blue: after the further addition of 2.0 eqs. of NaOH.

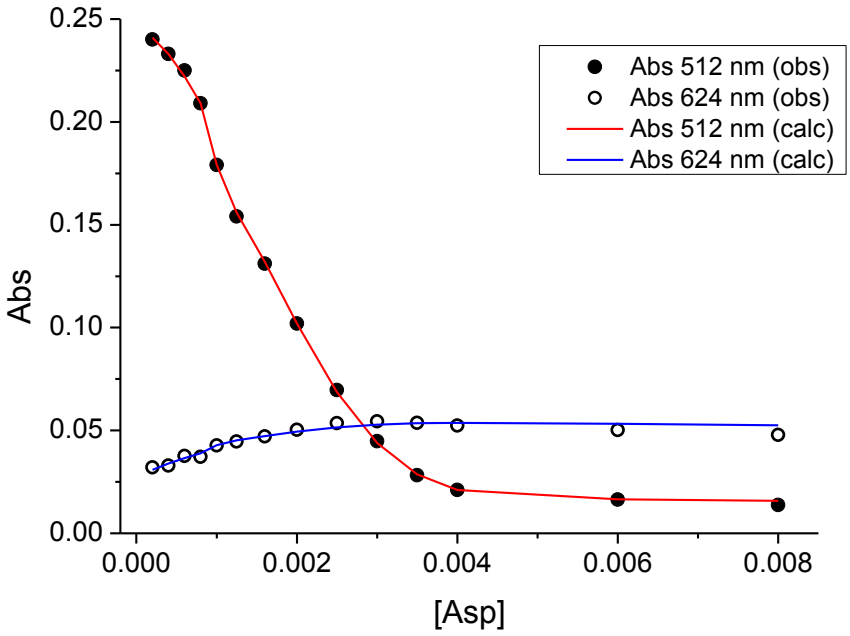

Figure S65. Absorbance values at 512 nm and 624 nm of Cu**L1** upon titration with $(TBA)_2$-L-Aspartate (symbols: experimental data; lines: fitted data).

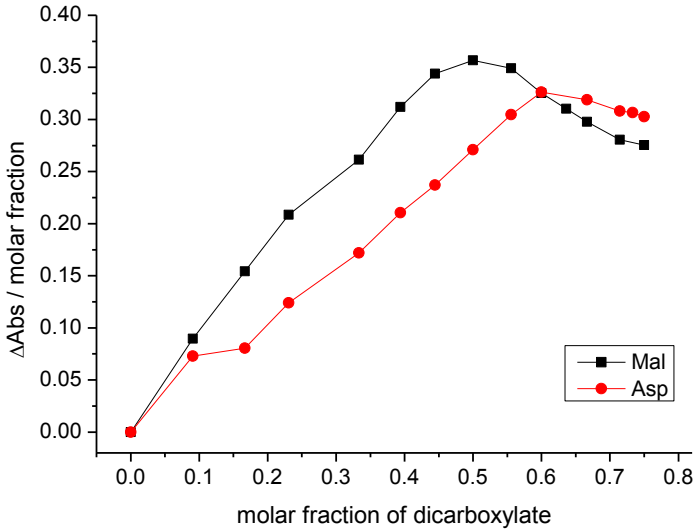

Figure S66. Job plots of the Cu**L1** - $(TBA)_2$-Aspartate system (in red) and of the Cu**L1** - $(TBA)_2$-Malate system (in black).

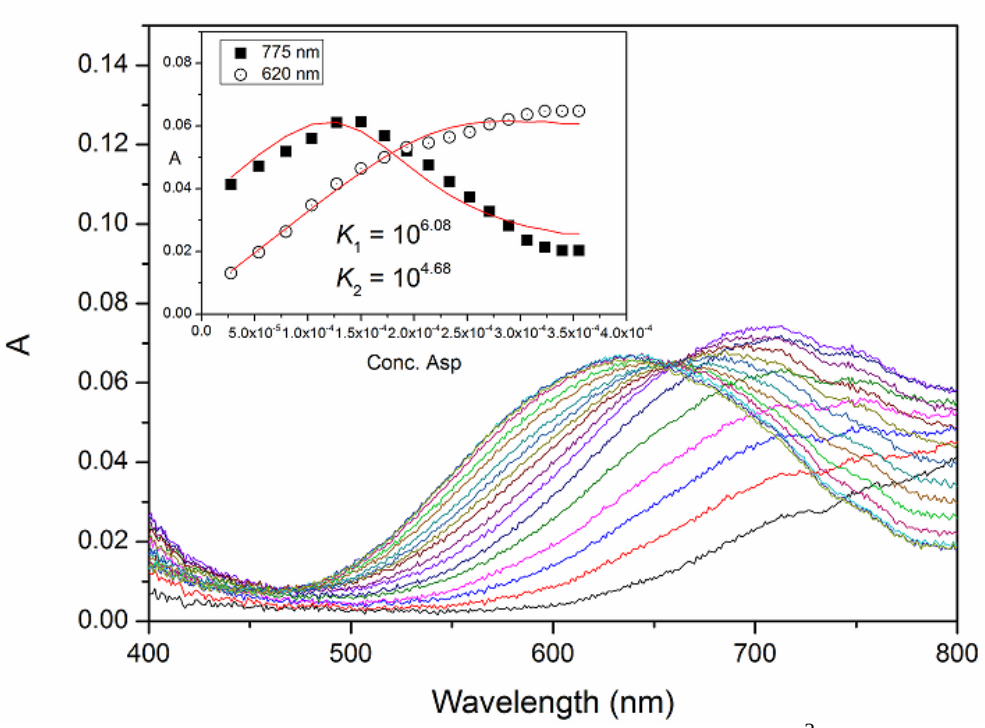

Figure S67. UV-vis spectral variations upon titration of $1.4 \cdot 10^{-3}$ M $CuSO_4$ with $1.4 \cdot 10^{-2}$ M $(TBA)_2$-L-Aspartate in MeOH. Inset: Absorption variations at 775 and 620 nm and fitting to the formation of the complexes CuAsp and $CuAsp_2$ with association constants $K_1 = 10^{6.08}$ M^{-1} and $K_2 = 10^{4.68}$ M^{-1}, respectively.

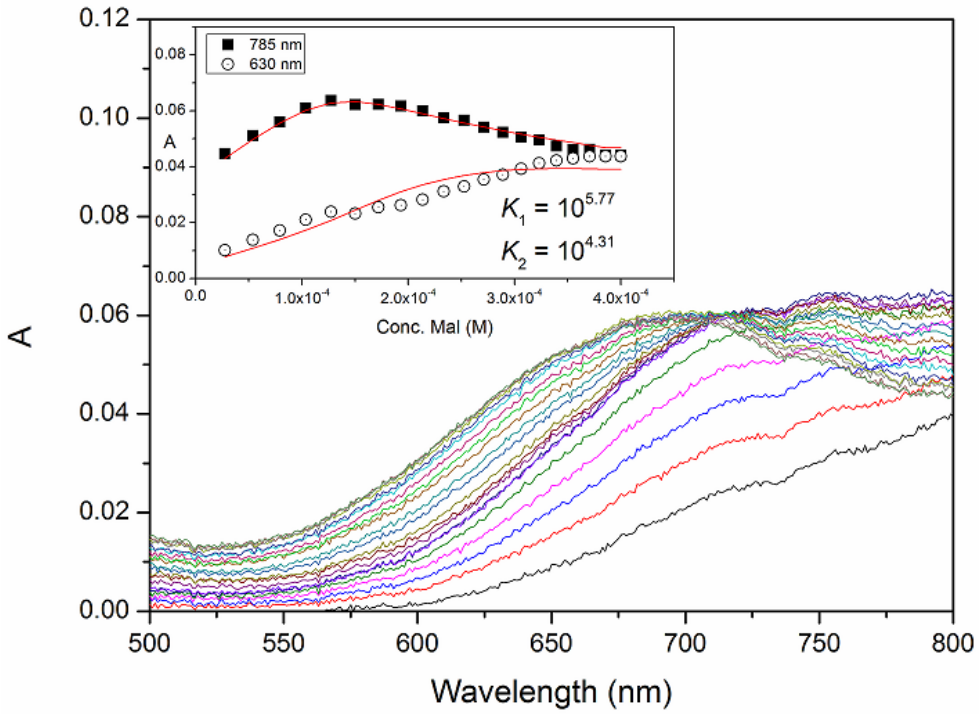

Figure S68. UV-vis spectral variations upon titration of $1.4 \cdot 10^{-3}$ M $CuSO_4$ with $1.4 \cdot 10^{-2}$ M $(TBA)_2$-L-Malate in MeOH. Inset: Absorption variations at 785 and 630 nm and fitting to the formation of the complexes CuMal and $CuMal_2$ with association constants $K_1 = 10^{5.77}$ M^{-1} and $K_2 = 10^{4.31}$ M^{-1}, respectively.

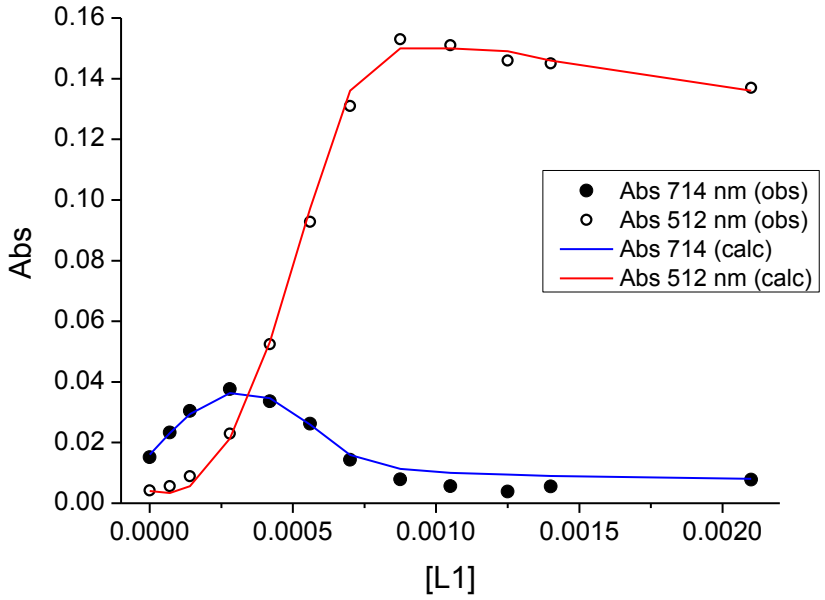

Figure S69. Absorbance values at 512 nm and 714 nm of $CuSO_4$ upon titration with **L1** in presence of stoichiometric amount of TBAOH (symbols: experimental data; lines: fitted data).

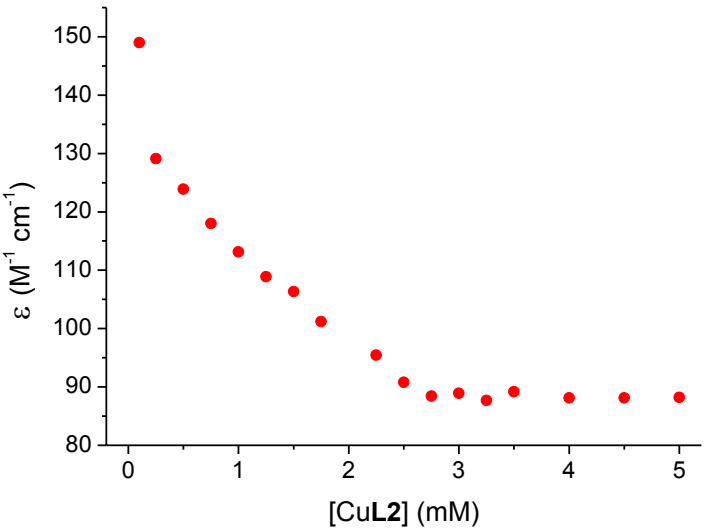

Figure S70. Dilution study of Cu**L2** in MeOH.

7. NMR spectra (Cu(II) complexes and dicarboxylates)

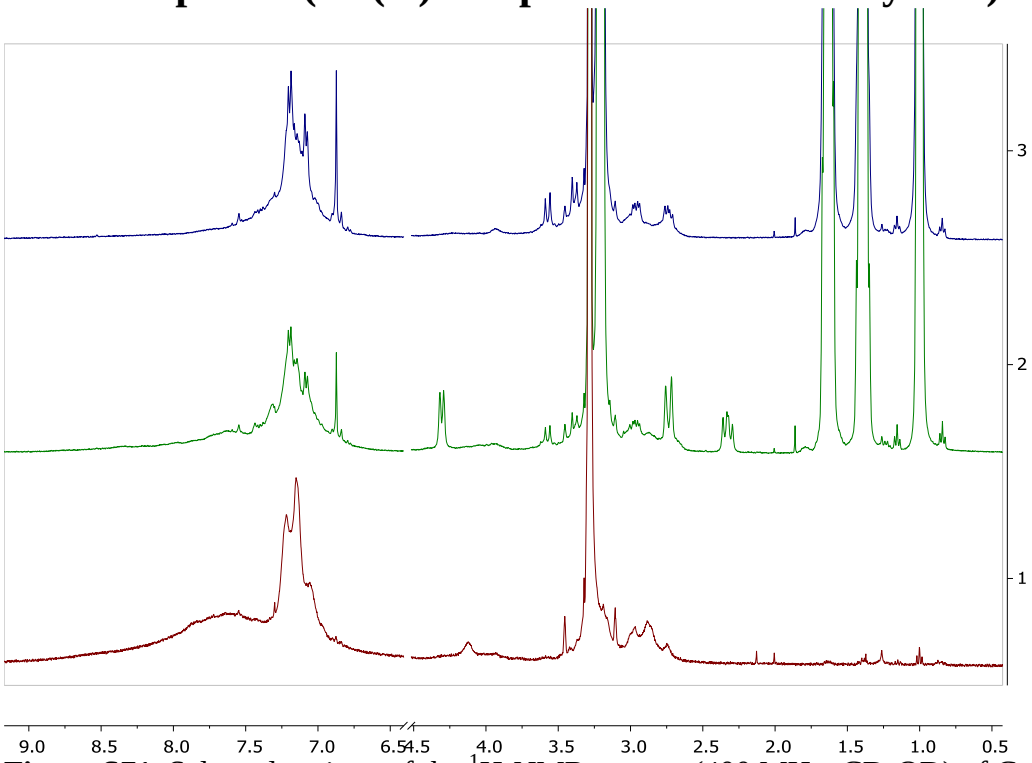

Figure S71. Selected regions of the ^{1}H-NMR spectra (400 MHz, CD_3OD) of Cu_2**L3** (bottom), Cu_2**L3** plus $(TBA)_2$-L-Malate (middle) and Cu_2**L3** plus $(TBA)_2$-L-Aspartate (top).

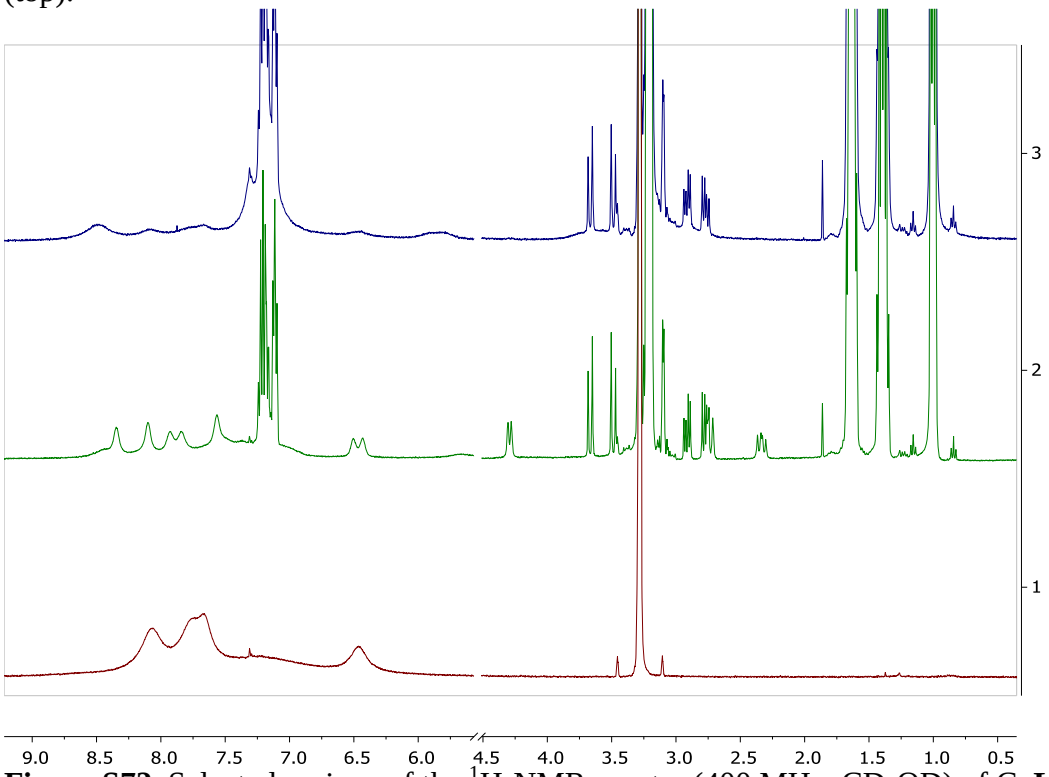

Figure S72. Selected regions of the ^{1}H-NMR spectra (400 MHz, CD_3OD) of Cu**L1** (bottom), Cu**L1** plus $(TBA)_2$-L-Malate (middle) and Cu**L1** plus $(TBA)_2$-L-Aspartate (top).